Chemical Engineering Science 310 (2025) 121570

Contents lists available at ScienceDirect

Chemical Engineering Science

journal homepage: www.elsevier.com/locate/ces

Trickle bed reactor technology for propylene epoxidation with extrudates – Catalyst characterization, kinetic studies and modelling

Christopher Stäglich [a,b], Matias Alvear [a,c], Christoph Schmidt [a], Ilari Angervo [d], Vincenzo Russo [a,e], Stefan Haase [b,f], Tapio Salmi [a,e,*]

[a] Åbo Akademi, Laboratory of Industrial Chemistry and Reaction Engineering (TKR), Turku FI-20500, Finland
[b] Technische Universität Dresden, Chemische Verfahrenstechnik, Dresden D-01069, Germany
[c] University of Wisconsin-Madison, Department of Chemical and Biological Engineering, 1415 Engineering Dr, Madison, WI 53706 United States
[d] University of Turku, Wihuri Physical Laboratory, FI-20014, Finland
[e] Universitá di Napoli 'Federico II', Chemical Sciences, Napoli IT-80126, Italy
[f] Hochschule für Technik und Wirtschaft Dresden, Verfahrenstechnik, Dresden DE-01069, Germany

ARTICLE INFO

Keywords:
Epoxide
Extrudate
Trickle bed
Kinetics
Transport phenomena
Modelling

ABSTRACT

Titanium silicate (TS-1) extrudates were prepared, characterized and tested in a trickle bed reactor (TBR) for selective epoxidation of propylene to propylene oxide. Hydrogen peroxide was used as the epoxidation agent. A preliminary study was conducted with extrudates with a diameters 1.5–3 mm. The smallest extrudate showed the highest propylene conversion and was used for an extensive screening of the reaction conditions (temperature, pressure, liquid and gas flow rates, composition of the educt solution). A dynamic multiphase reactor model was developed based on the steady state reaction kinetics approach. The internal mass transfer effects inside the extrudates were described with a reaction–diffusion model and the backmixing effects inside the catalyst bed were modelled with the axial dispersion concept. The mass balances of the components in the gas, liquid and solid catalyst phases were solved numerically with *gProms ModelBuilder*. The prediction of the model was for the most experimental data within +/- 10 %. The model was used to the simulate the concentration profiles of the participating molecules in time and space.

1. Introduction

The production of important fine and basic chemicals in an ecological friendly way is one of the acute challenges for the contemporary chemical industry. Epoxides of alkenes and fatty acids are important chemical intermediates which are used for environmentally friendly production of diols, polyols, bio-lubricants and polymers. In case of epoxide production, the epoxidation of alkenes with the aid of titanium silicate catalysts plays a very crucial role. The commercial propylene epoxidation catalyst TS-1 was launched in 1983 by the Italian enterprise ENI (Taramasso, 1983; Russo et al., 2013). The most important advantages of this epoxidation process are the mild reaction conditions, i.e. low temperature and low pressure, as well as a high epoxide selectivity; the appearance of harmful secondary by-products is suppressed in the presence of titanium silicate catalysts. This reaction pathway has been commercialized by Dow/BASF and Evonik/SKC (Russo et al., 2013; Bassler et al., 2010). The reaction system itself is principally simple. Propylene reacts with hydrogen peroxide to propylene oxide and, depending on the chemical environment, some by-products are formed because of ring opening as illustrated in Fig. 1. Methanol is a frequently used as the solvent in the epoxidation process and hydrogen peroxide is introduced to the system in form of an aqueous solution, thus promoting ring opening (Russo et al., 2013; Bassler et al., 2010; Alvear et al., 2023; Alvear et al., 2021; Liu et al., 2004; Alvear et al., 2022; Alvear et al., 2023; Azarpour et al., 2021; Influence of Si/Ti ratio and calcination conditions, 2024; Belussi et al., 1992; Bonino et al., 2004). The potential ring-opening products are 1-methoxypropan-2-ol (1-MP), 2-methoxypropan-1-ol (2-MP) and propylene glycol (PG), respectively. The reaction stoichiometry is not very complicated as such, but the reactor system is rather demanding since gas, liquid and solid phases always coexist in the system.

Trickle bed reactors are used for this epoxidation process, characterized by concurrent gas and liquid flows through the catalyst bed. By using trickle beds, the flow pattern of the liquid phase approaches plug flow, ensuring a high alkene conversion.

* Corresponding author.
E-mail address: tapio.salmi@abo.fi (T. Salmi).

https://doi.org/10.1016/j.ces.2025.121570
Received 21 October 2024; Received in revised form 10 March 2025; Accepted 19 March 2025
Available online 20 March 2025

Nomenclature

Latin letters

A	area
A	parameter related to catalyst shape
a_v	surface area-to-volume ratio
B	parameter in related to catalyst shape
C	concentration
D	diffusion coefficient, dispersion coefficient
d	diameter
E_A	activation energy
G	parameter for the estimation of molar volume
H	Henry's constant
K	adsorption equilibrium parameter
k	rate constant
k_L	liquid-phase mass transfer coefficient
k'	merged rate parameter
k'_0	merged rate parameter at reference temperature
L	length
M	molar mass
N	diffusion flux
n	exponent
P	pressure
R	general gas constant
r	reaction rate
s	shape factor
T	temperature
t	time
TOS	time-on-stream in continuous system ($=t$)
u	velocity
V	molar volume
X	Lockhart-Martinelli ratio
z	length coordinate

Greek letters

ε	porosity, hold-up
μ	dynamic viscosity
ν	stoichiometric coefficient
ξ	liquid–solid interface ratio
ρ	density
τ	tortuosity
ϕ	association factor, sphericity
χ	dimensionless length coordinate

Dimensionless numbers

Ga	Galilei number
Pe	Péclet number
Re	Reynolds number
Sc	Schmidt number
We	Weber number

Subscripts and superscripts

A	solute molecule
axial	axial parameter
B	solvent molecule
Cat	catalyst
eff	efficient property
G	gas
i	component index
j	reaction index
k	Kirscher-Kant (hydraulic diameter)
L	liquid
P	particle
ref	reference (temperature)
s	solid
v	area-to-volume
w	wetted area
0	reference condition

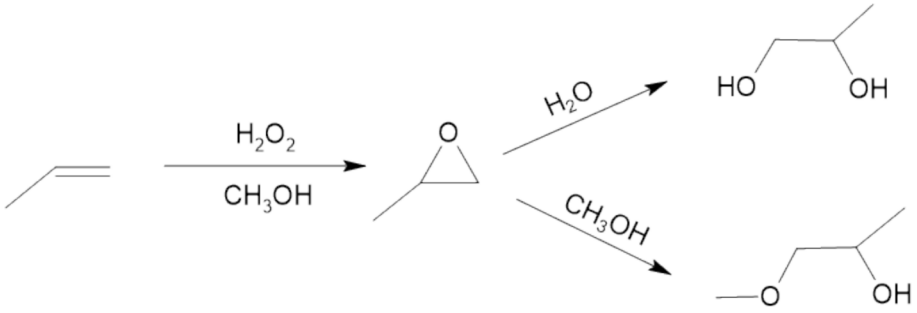

Fig. 1. Epoxidation of propylene with hydrogen peroxide in methanol.

In the classical monograph of Ranade et al. (Ranade et al., 2011), the performance of trickle bed technology is compared with other three-phase reactors, such as stirred slurry reactors, ejector loop reactors and bubble columns. The great benefits of trickle beds are that they enable continuous operation, high loading of solid catalysts, relatively low catalyst attrition. Trickle beds can operate within large temperature and pressure intervals and, if plug flow conditions are approached, the high conversion of reactants can be achieved for most type of kinetics, i. e. reaction orders higher than zero (Ranade et al., 2011; Al-Dahhan et al., 1997). Moreover, trickle beds are well adapted to process development: as new catalysts are discovered, they can replace the old ones in the same reactor. The size of catalyst particles can vary from millimeter scale to approx. 1–1.5 cm. Besides simple cylinders, more advanced catalyst particle shapes are available, such as trilobes, quadrilobes, wagon wheels and hollow cylinders. The very recent development of 3D printing technologies enables even more sophisticated particle design, to improve the local turbulence and diminishing the diffusion distance in the porous particle structure. The main challenges of trickle bed technology are related to the risks of flow maldistribution, partial wetting of the catalyst particles and strong mass transfer limitations at the gas–liquid and liquid–solid interfaces as well as inside the catalyst particles. The internal diffusion resistance can be suppressed by using small catalyst particles, which however increase the pressure drop in the reactor tube. The interaction between intrinsic reaction kinetics and mass transfer effects makes the design and modelling of trickle bed reactor systems challenging.

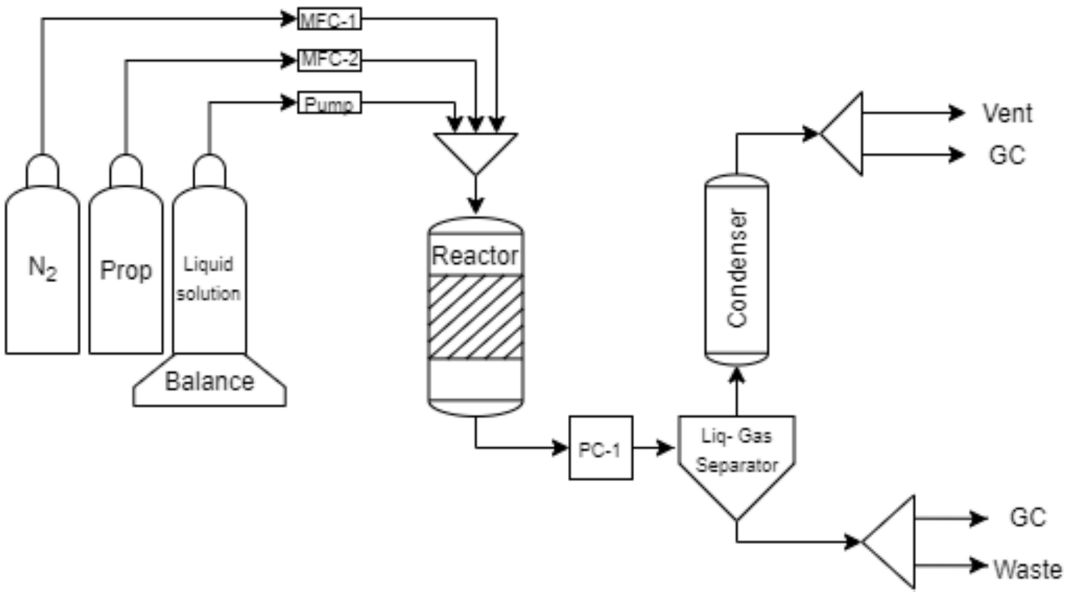

Fig. 2. Overview of the experimental setup for propylene epoxidation.

Table 1
Overview of the catalyst and reactor setup.

Properties of the setup	Value	Unit
D_i	15	mm
L	340	mm
$d_{Extrudate}$	1.5 – 3.0	mm
ρ_s	2.6	g/cm^3

Table 2
Calculation of the shape factor (s).

R_p [mm]	A_p [mm^2]	V_p [mm^3]	s [-]
0.75	60.08	21.21	1.125

Table 3
Molar volumes and diffusion coefficients at reference temperature 313.15 K.

Compound	V_A [cm^3/mol]	10^9 $D_{A,B}$ [m^2/s]
Propylene	68.8	3.15
H_2O_2	28.64	5.32
H_2O	18.39	6.94
Propylene oxide	69.57	3.12
1-MP	108.18	2.40
2-MP	108.10	2.40
Methanol	42.9	4.18

In spite of some disadvantages, trickle beds have preserved their position as one of the work horses of contemporary chemical and petrochemical industries. Ranade et al. (Ranade et al., 2011) have estimated that 1.6 billion t/y of chemical products are obtained with trickle bed reactors. Azarpour and co-workers (Azarpour et al., 2021) have published a comprehensive review on the performance analysis and modeling of catalytic trickle bed reactors. Trickle beds are applied in hydrogenation, hydrodesulphurization, hydrodemetalation, transesterification, halogenation and oxidation reactions. It is expected that trickle beds will in future get new markets thanks to the on-going green transition towards renewable raw materials, components from biomass, such as chemical transformation of sugars, extractives, fatty acids and lignin to valuable chemicals, fuel components and food ingredients. An important application of trickle beds is related to environmental technology, particularly catalytic oxidation of pollutants (Azarpour et al., 2021).

Concerning the mathematical modelling of trickle beds, several approaches have been proposed and applied to real cases. The simplest models are pseudo-homogeneous ones, i.e. the reactor content is regarded as a continuum and, if deviations from plug flow are expected, they are described with the concept axial dispersion (Péclet number). Particularly for strongly exothermic or endothermic reactions, it is necessary to include the energy balances and typically also the radial dispersion effects, which requires a two-dimensional model. However, pseudo-homogeneous models are strongly limited, because the interfacial and intraparticular transport phenomena are often prominent and should be explicitly included in the model. Shifting from pseudo-homogeneous to heterogeneous models implies the inclusion of gas–liquid and liquid–liquid mass and heat transport effects as well as the diffusion of heat and mass inside the catalyst particles. The approach of dynamic (time dependent) heterogeneous models is described in detail in the review article (Azarpour et al., 2021). With the current computational tools, the numerical solution of this kind of model is fully feasible, as has been illustrated, for example by Russo et al. (Russo et al., 2015), and Hachhach et al (Hachhach et al., 2023), where the gPROMS software was successfully used. The most advanced modelling approach implies the use of Navier-Stokes equations to reveal the detailed flow pattern around the catalyst particles. With the available tools for Computational Fluid Dynamics (CFD) the mesoscale flow models based on the unit-cell approach can be solved numerically (Ranade et al., 2011), but the coupling of this kind of modelling to the reaction–diffusion model leads very demanding computations on the reactor level. This can become an obstacle, particularly if the model is used for parameter estimation, which requires hundreds, even thousands of model simulations to find the optimal set of parameters.

In previous studies of propylene epoxidation, the transport phenomena have been discarded because the work has been focused on the performance of finely dispersed powder catalysts (Alvear et al., 2022; Alvear et al., 2023). However, for continuous operation and process scale-up, it is important to consider larger catalyst particles and packed bed reactors. The main goal of the present work is to investigate the coupling between intrinsic reaction kinetics and transport phenomena on catalyst particles in a laboratory-scale trickle bed reactor.

The effect of the extrudate diameter on the epoxidation performance was investigated in the first stage, after which the reaction conditions were screened to reveal the impact of temperature, pressure,

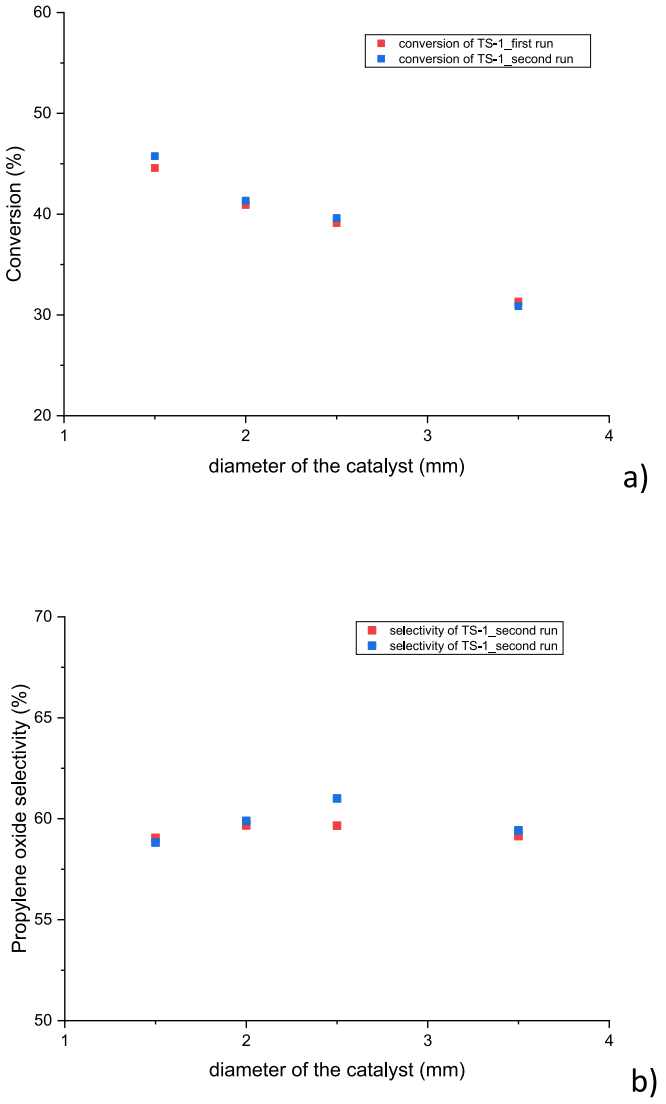

Fig. 3. Dependence of propylene conversion (a) and propylene oxide selectivity (b) on the diameter of the TS-1 catalyst extrudates.

Table 4
Nitrogen physisorption results.

Sample	Surface area [m^2/g]	Meso-porous volume [cm^3/g]	Median pore diameter [nm]	Microporous volume [cm^3/g]
TS-1_1.5 mm_fresh	418	0.118	0.617	0.202
TS-1_1.5 mm_spent	223	0.033	0.626	0.104
TS-1_2 mm_fresh	309	0.035	0.615	0.154
TS-1_2 mm_spent	281	0.063	0.618	0.136
TS-1_2.5 mm_fresh	259	0.133	0.625	0.126
TS-1_2.5 mm_spent	262	0.052	0.629	0.126
TS-1_3 mm_fresh	291	0.028	0.624	0.140
TS-1_3 mm_spent	270	0.047	0.625	0.133

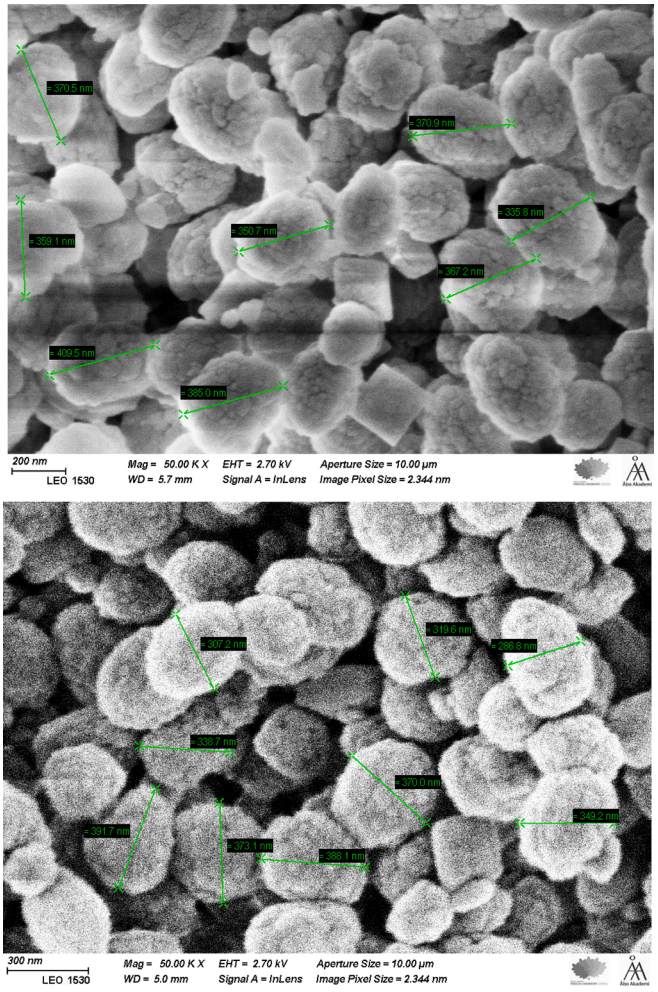

Fig. 4. Comparison of SEM images of fresh (upper) and spent extrudates (lower).

Table 5
Results from EDS measurements.

Sample	Amount of SiO_2 [wt.%]	Amount of TiO_2 [wt.%]	Molar Si/Ti ratio [-]
TS-1_1.5 mm_fresh	81.93	17.82	6.11
TS-1_1.5 mm_spent	81.31	18.69	5.78
TS-1_2 mm_fresh	81.86	18.14	6.00
TS-1_2 mm_spent	82.26	17.27	6.32
TS-1_2.5 mm_fresh	81.21	18.79	5.75
TS-1_2.5 mm_spent	81.98	18.02	6.05
TS-1_3 mm_fresh	81.41	18.59	5.82
TS-1_3 mm_spent	84.57	15.43	7.29

composition of the educt solution and fluid flow rate on the reactant conversion and product selectivity. An advanced multiphase reactor model was implemented to study the behavior of the system under various operation conditions.

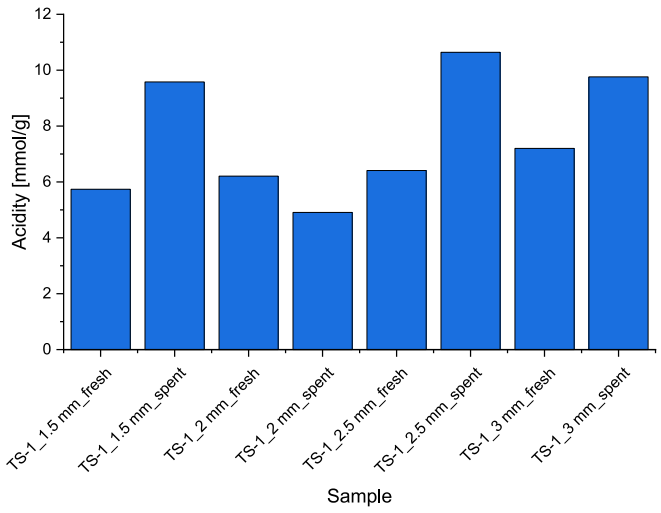

Fig. 5. TPD measurement results of extrudates.

2. Experimental section

2.1. Chemicals and materials

The gases were propylene (AGA) and nitrogen (Woikoski). Hydrogen peroxide (30 wt%, Sigma Aldrich) and highly pure methanol (>99.9 wt %, Sigma Aldrich) were used in the trickle bed experiments. Propylene glycol (<99.5 %, Sigma Aldrich), propylene oxide (99.9 %, Sigma Aldrich), 1-methoxy-2-propanol (>99.5 %, Sigma-Aldrich) were used to calibrate the gas chromatographic analysis. The catalyst was a commercial titanium-silicate (TS-1) of ACS material type B (CAS No 13463–67-7 (titanium dioxide) and 7621–86-9 (silicon dioxide)). The catalyst powder was extruded without a binder and shaped to extrudates with 1.5 mm, 2 mm, 2.5 mm and 3 mm diameters.

2.2. Catalyst characterization methods and procedures

The TS-1 catalyst extrudates were used in preliminary experiments, to investigate the impact of the catalyst diameter (catalyst layer thickness) on the internal diffusion in the pores. The catalyst extrudates were characterized by different solid analysis methods before and after the reaction experiments.

The specific surface area, pore volume and pore distribution were measured with nitrogen physisorption (Micrometrics 3 Flex equipment). The samples were pretreated in two steps before starting the measurement. To remove adsorbed gases from air, the samples were pretreated at 180 °C and 0.1 mbar *ex situ* degassing for 24 h. Afterwards, *in situ* degassing was carried out for 6 h at 180 °C and 0.05 mbar. After the measurement, the specific surface area was calculated with the Dubinin-Radushkevich method. The pore size distribution and the pore volumes were estimated with the aid of the density functional theory (DFT).

The acidity of the catalyst material was analyzed with temperature programmed desorption (TPD). The knowledge of the acidity is important, because the titanium metal provides the active sites for chemical reactions. Ammonia was the probe molecule in the TPD. The samples were pretreated with 500 °C, whereby a heating rate of 25 °C /min was used and the temperature was maintained for 60 min under a helium flow of 30 ml/min. Subsequently, the sample was cooled down to 100 °C. After the desired temperature had been reached, a gas mixture with 5 % NH_3/He was dosed for 30 min. The sample was flushed with helium for 60 min to cool down to 50 °C. For the desorption process, the target temperature was set to 600 °C and reached with a heating rate of 10 °C /min. This temperature was kept for 20 min. The outlet gases were monitored with a thermal conductivity detector (TCD).

For analyzing the morphological features such as the textures and shapes of the crystals, the materials were investigated with scanning electron microscopy (SEM, Zeiss Leo Gemini 1530). X-ray diffraction (XRD) was used to analyze the structure, phase purity and crystallinity. The instrument for the investigation was a PANalytical Empryean diffractometer with a five-axis goniometer. The X-ray radiation was filtered to comprise the Cu $K_{\alpha1}$ and Cu $K_{\alpha2}$ radiations only.

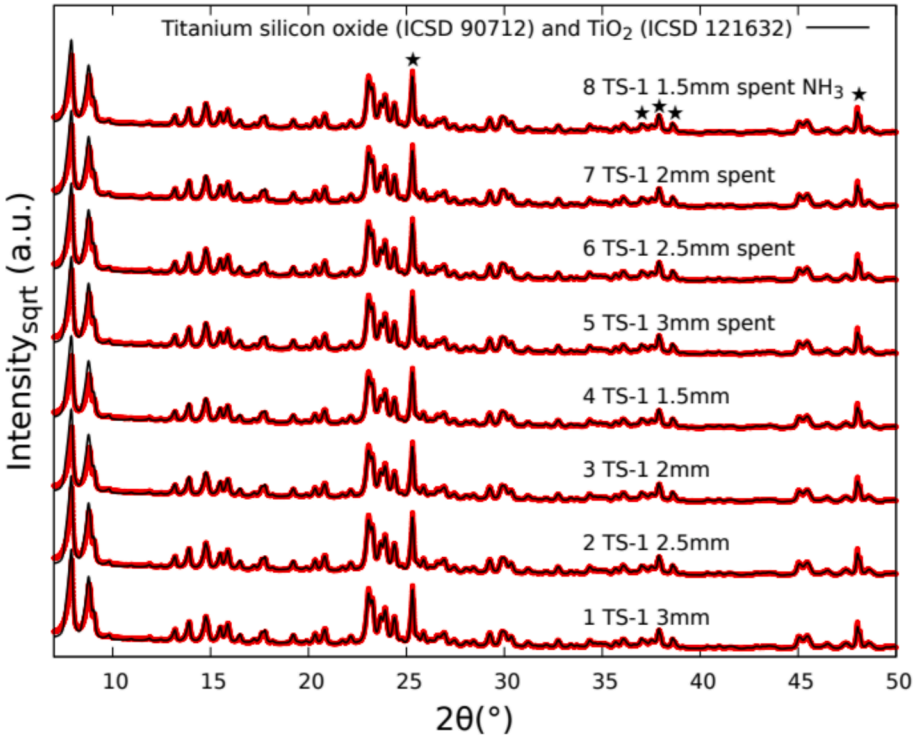

Fig. 6. XRD diffractograms in the range of θ from 5° to 120°.

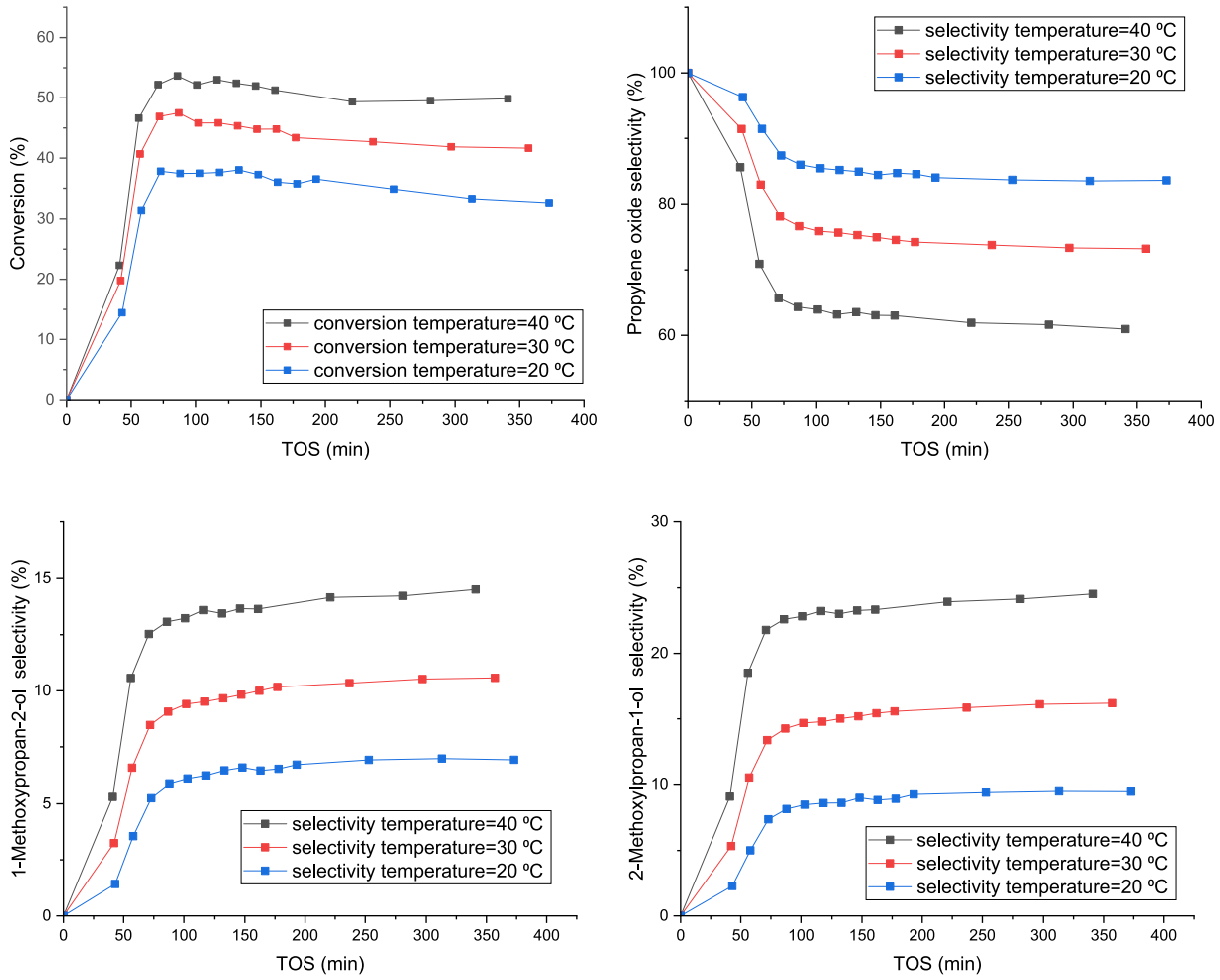

Fig. 7. Effect of reaction temperature on propylene conversion and product selectivity. Reaction conditions: P = 4.5 bar; liquid flow rate = 0.5 ml/min; gas flow rate = 5 ml/min; wt.% H_2O_2 = 2.

2.3. Experimental equipment and product analysis

The experimental setup is described in the previous investigations of our group (Alvear et al., 2023; Alvear et al., 2021; Alvear et al., 2022; Alvear et al., 2023). The most important elements of the equipment are summarized in Fig. 2. The reactor tube had the diameter of 15 mm and length of 340 mm. The catalyst bed was placed in the lower part of the reactor and consisted of 1 g TS-1 extrudates and 20 g quartz sand (>125 μm) to avoid the appearance of hot spots and to promote local turbulence inside the bed. The upper part of the reactor was filled with quartz sand to get good backmixing of the gas and liquid phases. The basic catalyst structure and the reactor setup are summarized in Table 1.

For the liquid-phase feed, a mixture of methanol, hydrogen peroxide and water was produced. The amount of hydrogen peroxide depended on the actual experimental conditions. Nitrogen and propylene were flowing inside the reactor tube concurrently and the flow rate of propylene was varied in the experiments. While the gas flow rates were regulated by mass flow controllers, a high-performance liquid chromatography (HPLC) pump (Agilent 1100 series) was used to feed the liquid phase into the system.

For the pressure control (PC-1) a Equilibar (U3L Ultra Low Flow Back Pressure Regulator) was utilized. With the aid of a condenser operating at 0ºC, the gas and liquid phases were separated. The product analysis was accomplished by two gas chromatographs, an online chromatograph for the gas phase (Agilent Micro GC 990) and an offline one for the liquid phase (Agilent 6890 N).

The liquid phase was analyzed with a capillary column (Plot U and Molsieve) with a length of 60 m, a diameter of 530 μm and an active phase thickness of 20 μm. The operation temperature was 185 ºC. The micro gas chromatograph for the gas analysis was equipped with Molsieve and PoraPlot columns, where only the PoraPlot Unit was used. The micro gas chromatograph was calibrated with nitrogen, propylene and a mixture relevant for the reaction conditions. For the calibration of the liquid phase, propylene oxide, propylene glycol and 1-methoxy-2-propanol with the amounts of 5, 2.5, 1.25 and 0.625 wt% were used. The concentration responses were linear with respect to the peak areas observed in the chromatograms.

2.4. Preliminary investigation of extrudates

To reveal the effect of internal diffusion on the epoxidation process, four extrudates were investigated: the catalyst particle diameters were 1.5 mm, 2.0 mm, 2.5 mm and 3.0 mm. The experiments were repeated twice under identical conditions listed in Supporting Information (SI).

2.5. Systematic kinetic studies and characterization of fluid dynamics

The kinetic and mass transfer studies included step response experiments with different gas and liquid flow rates, different amounts of hydrogen peroxide and water, as well as different pressures and temperatures. The large amount of data was mandatory to estimate all the parameters included in the mathematical model. An overview of the reaction conditions is provided in Supporting Information (SI).

To avoid explosive gas mixtures of propylene and oxygen, the reactor

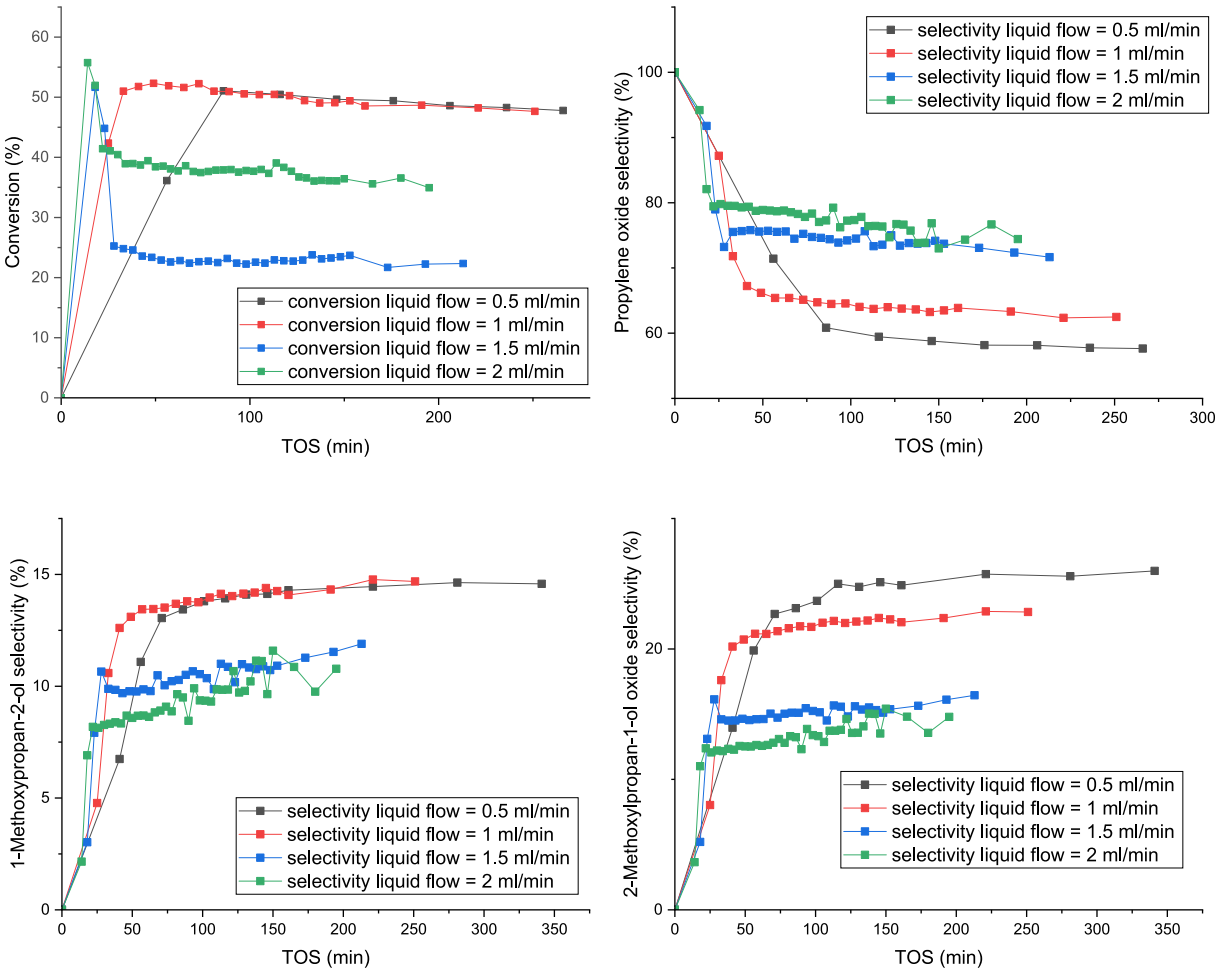

Fig. 8. Effect of liquid flow rate on propylene conversion and product selectivity. Reaction conditions: P = 4.5 bar; T = 40 °C; gas flow rate = 5 ml/min; wt.% H_2O_2 = 2.

system was flushed with nitrogen prior to each experiment. After the experiment, the reactor system was cleaned by flushing it for two hours with pure methanol to remove leftovers of hydrogen peroxide and secondary reaction products (Fig. 1). During this cleaning period, the temperature was set to 70 °C and the pressure was increased up to 6.5 barg.

3. Mathematical modelling

3.1. Background

Quite few mathematical models have been published on propylene epoxidation. Danov et al. investigated extruded TS-1 catalysts in a fixed bed reactor (Russo et al., 2015). The temperature was varied between 30 °C and 60 °C and the pressure was 5–7 bar. The catalyst itself was made by the TS-1 powder, which was extruded with aluminum 5,6-oxynitrate as the binder. The reaction was investigated with methanol as solvent. Another study concerning the epoxidation kinetics has been published by Russo et al. (Russo et al., 2014). The main aim of the work was to investigate the impact of temperature, pressure, catalyst amount, and amount of hydrogen peroxide. At the end of the study, a kinetic model was proposed to describe the experimental data, generated from a batch reactor. Recently more advanced studies have been published. Alvear et al. (Alvear et al., 2022; Alvear et al., 2023) proposed a model of the epoxidation process with small TS-1 catalyst particles in a laboratory-scale trickle bed reactor and Aquino et al. (Aquino et al., 2023) developed a mathematical model based on spatially resolved measurements.

The modeling approach presented is this article is somewhat different from previous studies (Alvear et al., 2022; Alvear et al., 2023). Preliminary investigations with the existing model obtained from Alvear et al. (Alvear et al., 2022) showed high deviations from the current experimental data, because profound mass transfer effects appeared in the extrudates. Therefore, a reaction–diffusion model was developed for the extrudates and this model was coupled to the gas- and liquid-phase mass balance equations of the components in the reactor bed.

3.2. Rate equations for propylene epoxidation and ring-opening

The chemical system can be characterized as a combination of consecutive and parallel reactions as sketched in Fig. 1. Therefore, following to the epoxidation of propylene (Pr) to propylene oxide (PO), the solvolysis of PO with water (W) and methanol (MA) to propylene glycol (PG) and methoxypropanols (1-MP and 2-MP) can appear as side reactions.

The reaction of propylene on the active sites of TS-1 in the presence of H_2O_2 has been investigated previously, and it is generally accepted that the formation of a titanium hydroperoxide species is the most important step in the epoxidation mechanism (Alvear et al., 2023; Danov et al., 2013; Russo et al., 2014). For the mechanistic approach, it is necessary to consider the dissociative adsorption of hydrogen peroxide, as the Ti-OSi bond is split leading to the formation of the Ti-OOH species. This species is stabilized by the protic solvent methanol (Alvear et al., 2022; Wu et al., 2008; van der Waal and van Bekkum, 1997; Corma et al., 1996).

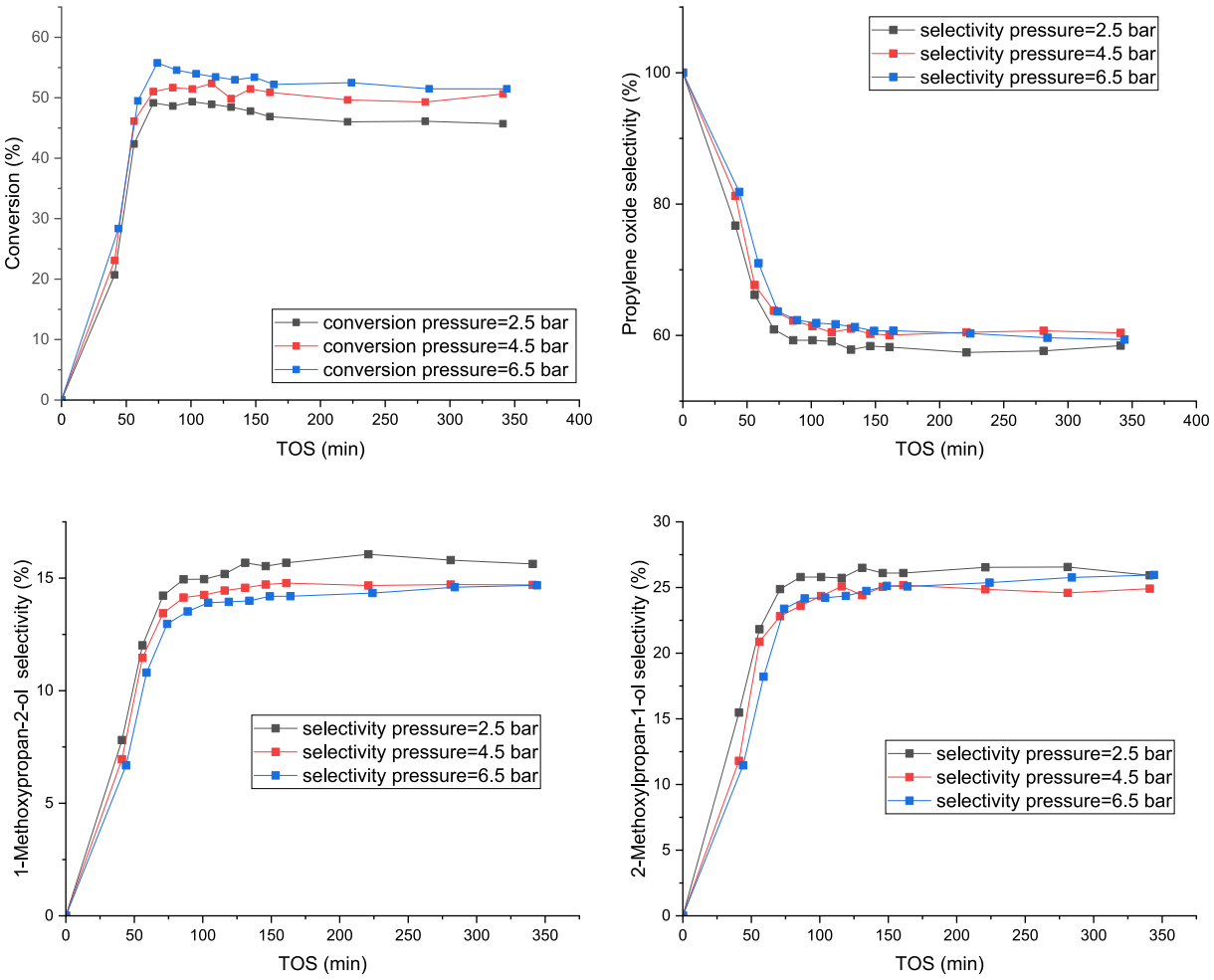

Fig. 9. Effect of pressure on propylene conversion and product selectivity. Reaction conditions: T = 40 °C; liquid flow rate = 0.5 ml/min; gas flow rate = 5 ml/min; wt.% H_2O_2 = 2.

Basically, the surface reactions leading to the formation of propylene oxide (PO) and the main ring-opening products 1-methoxypropan-2-ol (1-MP), 2-methoxylpropan-1-ol (2-MP) are.

$$C_3H_{6(s)} + H_2O^*_{2(s)} \xrightarrow{r1} C_3H_6O^*_{(s)} + H_2O_{(l)}(PO) \quad (1)$$

$$C_3H_6O^*_{(s)} + CH_3OH_{(l)} \xrightarrow{r2} C_4H_{10}O_{2(l)}(1-MP) \quad (2)$$

$$C_3H_6O^*_{(s)} + CH_3OH_{(l)} \xrightarrow{r3} C_4H_{10}O_{2(l)}(2-MP) \quad (3)$$

The decomposition of hydrogen peroxide is not considered because of the mild conditions; the decomposition takes place at temperatures exceeding 55 °C (Alvear et al., 2021). The appearance of propylene glycol (PG) is neglected in the model because of the very minimal amounts of PG formed.

The development of the rate equations is now based on the following hypotheses:

- The catalyst surface is homogeneous from the energetic viewpoint.
- The adsorption of propylene and water onto the catalyst surface can be neglected.
- The main reaction takes place between hydrogen peroxide adsorbed on the catalyst surface and the olefin in the liquid phase (Eley-Rideal mechanism).
- The rate-limiting steps are the irreversible surface reactions (1)-(3).
- Side reactions giving the ring-opening products proceed on the catalyst surface.
- The adsorption–desorption steps of propylene oxide and hydrogen peroxide are rapid compared to the surface reactions, so the concept of adsorption quasi-equilibria can be applied on these steps.

Based on these hypotheses, the rate equations can be expressed as

$$r_1 = \frac{k_1 K_{HP} C_{HP} C_{Pr}}{1 + K_{HP} C_{HP} + K_{PO} C_{PO}} \quad (4)$$

$$r_2 = \frac{k_2 K_{PO} C_{PO} C_{MA}}{1 + K_{HP} C_{HP} + K_{PO} C_{PO}} \quad (5)$$

$$r_2 = \frac{k_3 K_{PO} C_{PO} C_{MA}}{1 + K_{HP} C_{HP} + K_{PO} C_{PO}} \quad (6)$$

where k_1, k_2, k_3 are the rate constants of the surface reaction steps and K_{HP} and K_{PO} denote the adsorption equilibrium parameters of hydrogen peroxide and propylene oxide.

To suppress the correlation between the kinetic and adsorption constants in the parameter estimation, merged parameters (k'=k_j K_l), where j = 1,2 or 3 and l=HP or PO) were introduced in the rate equations

$$r_1 = \frac{k'_1 C_{HP} C_{Pr}}{1 + K_{HP} C_{HP} + K_{PO} C_{PO}} \quad (7)$$

$$r_2 = \frac{k'_2 C_{PO} C_{MA}}{1 + K_{HP} C_{HP} + K_{PO} C_{PO}} \quad (8)$$

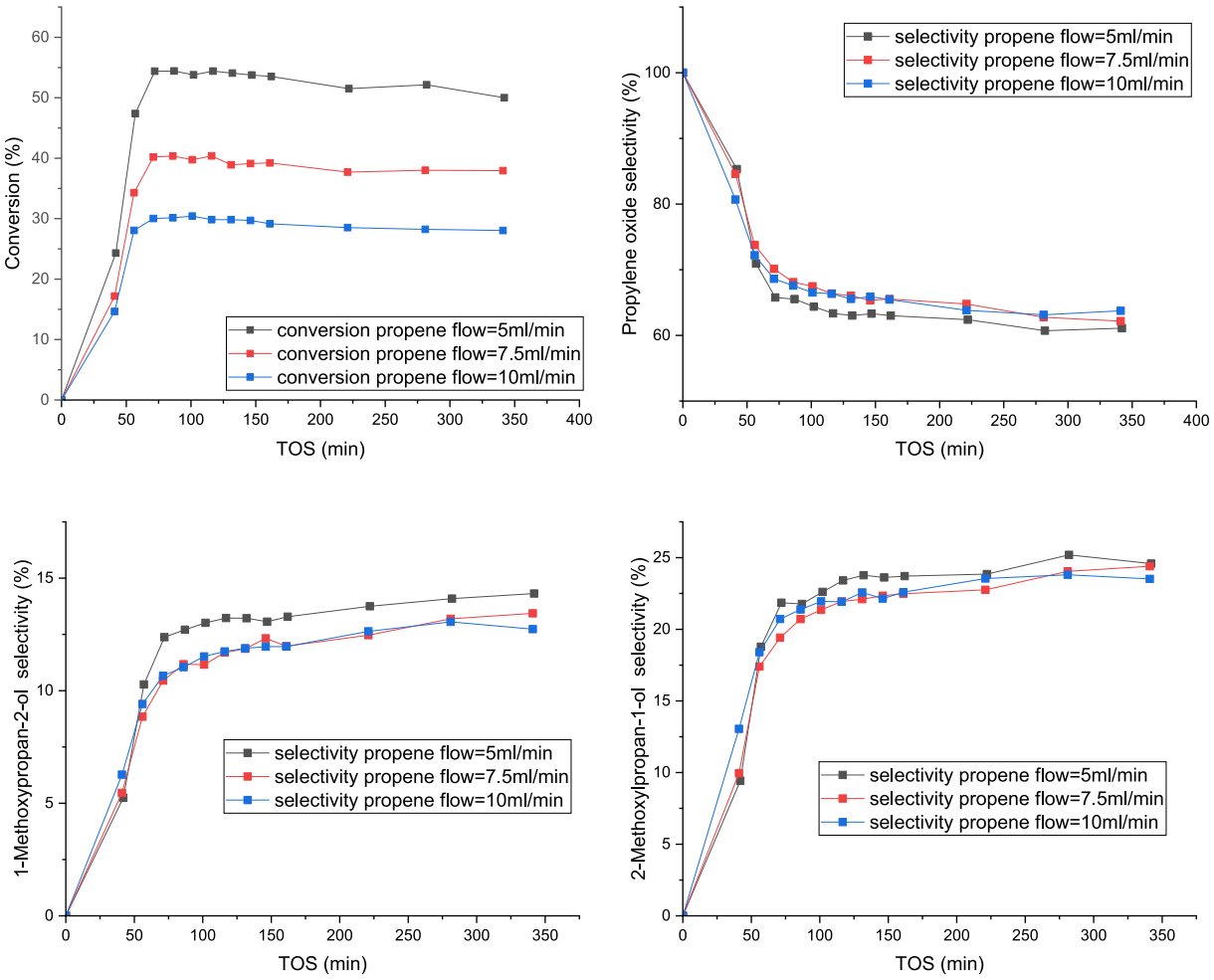

Fig. 10. Effect of propylene flow rate on propylene conversion and product selectivity. Reaction conditions: P = 4.5 bar; T = 40 °C; liquid flow rate = 0.5 ml/min; wt. % H_2O_2 = 2.

$$r_3 = \frac{k'_3 C_{PO} C_{MA}}{1 + K_{HP} C_{HP} + K_{PO} C_{PO}} \tag{9}$$

The temperature dependence of the kinetic constants is described with the modified Arrhenius law,

$$k'_j = k'_{0,j}[\exp\left(-\frac{E_{A,j}}{R}\left(\frac{1}{T} - \frac{1}{T_{ref}}\right)\right)] \tag{10}$$

The reference kinetic constant k'_0 is calculated at a chosen reference temperature T_{ref}. The gas constant is R (8.3143 J/(Kmol)) and the activation energy is E_A (J/mol). The modified Arrhenius law is used to minimize the correlation between the activation energy and the pre-exponential factor.

3.3. Trickle bed model

Basic hypotheses.

The trickle bed reactor model is basically a dynamic isothermal model for the three-phase system used in the experimental work. For the description of all the phenomena, it is necessary to describe the mass transfer between the gas and liquid phases, as well as between the liquid and the solid phases.

In accordance with previous investigations, the following fundamental assumptions are used in the model development (Alvear et al., 2022; Alvear et al., 2023):

I. Uniformity of the catalytic bed and the extrudates
II. Isothermal conditions
III. Negligible radial dispersion in the bed
IV. Axial dispersion model for the description of deviations from plug flow
V. Negligible radial temperature and concentration gradients
VI. Dynamic, time dependent model equations

In addition, it was possible to define the flow regime during the operation as the trickle flow regime with the aid of the empirical flow map published by Dudukovic and co-workers (Dudukovic et al., 2014). Several semi-empirical correlations are needed in the reactor model.

Hold-ups.

The solid hold-up ε_s can be calculated by the approach according to equation (11) and is basically related to the bed porosity ε_B,

$$\varepsilon_S + \varepsilon_B = 1 \tag{11}$$

The bed porosity ε_B is obtained from the empirical equation proposed by Pushnov (Pushnov, 2006);

$$\varepsilon_B = \frac{A}{\left(\frac{d_R}{d_p}\right)^n} + B \tag{12}$$

where A, B and n are parameters related to the catalyst shape. For the cylindrical extrudates A = 0.9198, B = 0.3414 and n = 2. This approximation is valid, because the ratio between the tube diameter (D)

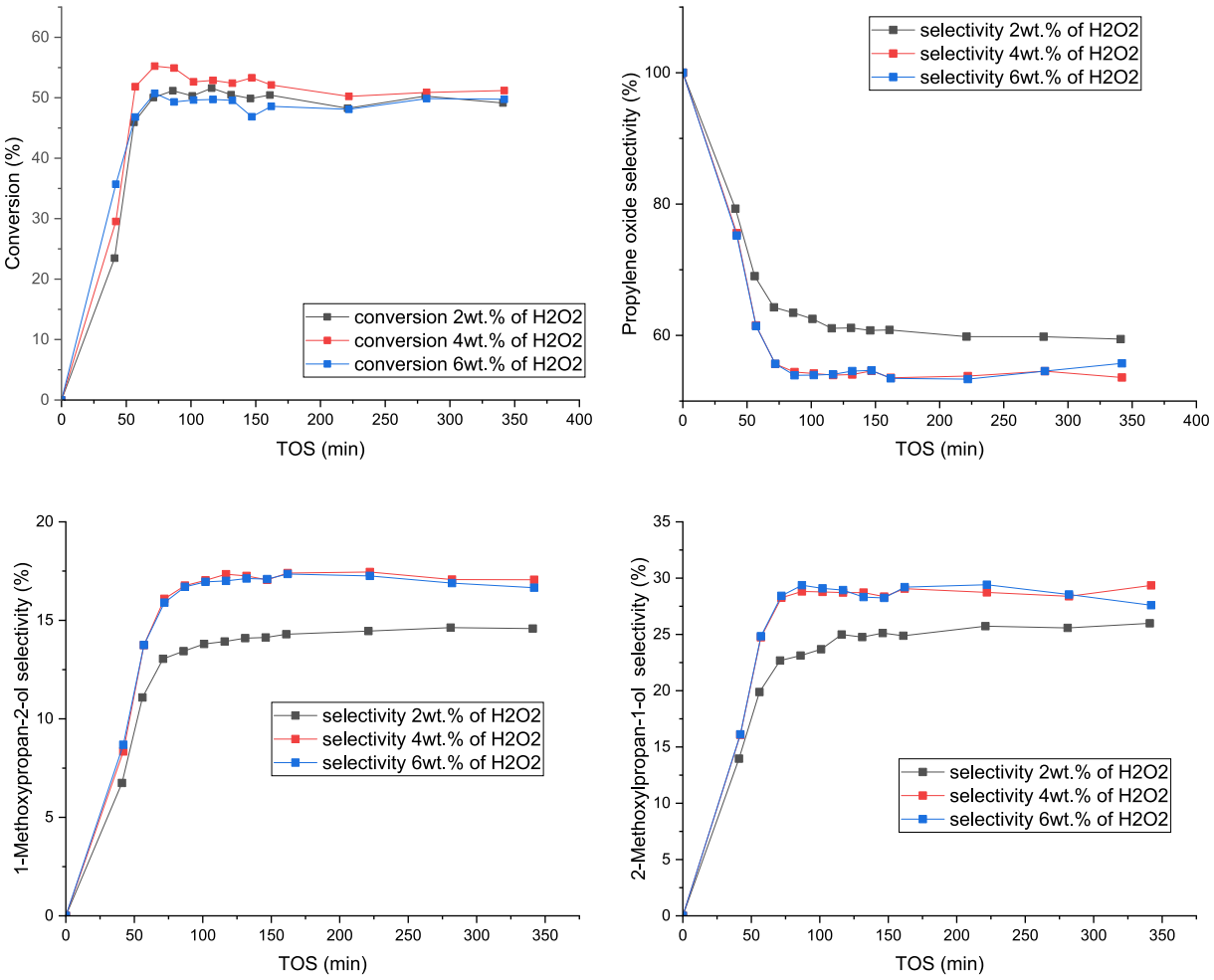

Fig. 11. Effect of hydrogen peroxide concentration on propylene conversion and product selectivity. Conditions: P = 4.5 bar; T = 40 °C; liquid flow rate = 0.5 ml/min; gas flow rate = 5 ml/min.

and the diameter of the catalyst extrudate is > 2. The catalyst bed is more than twenty times larger than the diameter. The value of the bed porosity is $\varepsilon_B = 0.34$. Consequently, the solid holp-up$\varepsilon_S = 0.65$. This value is reasonable with the consideration that the whole reactor tube is basically filled with solid material.

For the estimation of the liquid hold-up, the approximation (13) of Lange et al. (Lange et al., 2005) is used because it is valid for the very low flow rates,

$$\varepsilon_L = 0.16\left(\frac{d_R}{d_P}\right)^{0.33} Re_L^{0.14} \tag{13}$$

For the reference case (40 °C, 0.5 ml/min liquid flow, 5 ml/min propylene flow and 4.5 bar), the calculated liquid hold-up is approximated to 0.25. This value seems reasonable in comparison to the literature and similar reactor set-ups (García-Serna et al., 2017). The gas hold-up is obtained from

$$\varepsilon_G = 1 - \varepsilon_L - \varepsilon_S \tag{14}$$

giving$\varepsilon_G = 0.10$.

Gas-phase mass balance.

The mass balance of the gaseous phase can be described by equation (15),

$$\varepsilon_G \frac{\partial C_{i,G}}{\partial t} = -\frac{u_G}{L}\frac{\partial C_{i,G}}{\partial \chi} + \frac{\varepsilon_G}{Pe_G L}\frac{\partial^2 C_{i,G}}{\partial \chi^2} - N_{GL} a_{GL} \tag{15}$$

The concentrations of the gas-phase components $C_{i,G}$ are dependent on the convection, the axial dispersion and the gas–liquid mass transfer terms in the balance equation, where u_G is the gas-phase velocity and χ is the dimensionless axial coordinate calculated from axial coordinate (z) and the reactor length (L): $\chi = z/L$. N_{GL} describes the gas–liquid flux and a_{GL} is the parameter for the gas–liquid interfacial area. The gas–liquid flux is obtained from the law of Fick and the two-film theory, giving the simple expression

$$N_{GL} = \frac{C_{i,G} - HC_{i,L}}{\frac{H}{k_L}} \tag{16}$$

where H is the Henry's constant and k_L is the liquid-phase mass transfer coefficient.

To describe the phase equilibria for the estimation of the Henry's constant, the extended Soave-Redlich-Kwong (SRK) equation of state was used because of the presence of light olefins and the amount of water (Alvear et al., 2022; Alvear et al., 2023; T. Chang, R. M. Rousseau, and J. K. Ferrell, Vapor/liquid equilibria of constituents from coal gasification in refrigerated methanol, United States Environmental Agency, EPA/600/7-87/004, 1987). This equation was modified for the calculation of Henry's constant under the actual reaction conditions.

For the calculation of the merged gas–liquid mass transfer coefficient $k_L a_L$, equation (17) proposed by Ellman was used, which is valid for the trickle flow regime (Gianetto and Specchia, 1992; Ellman, 1988).

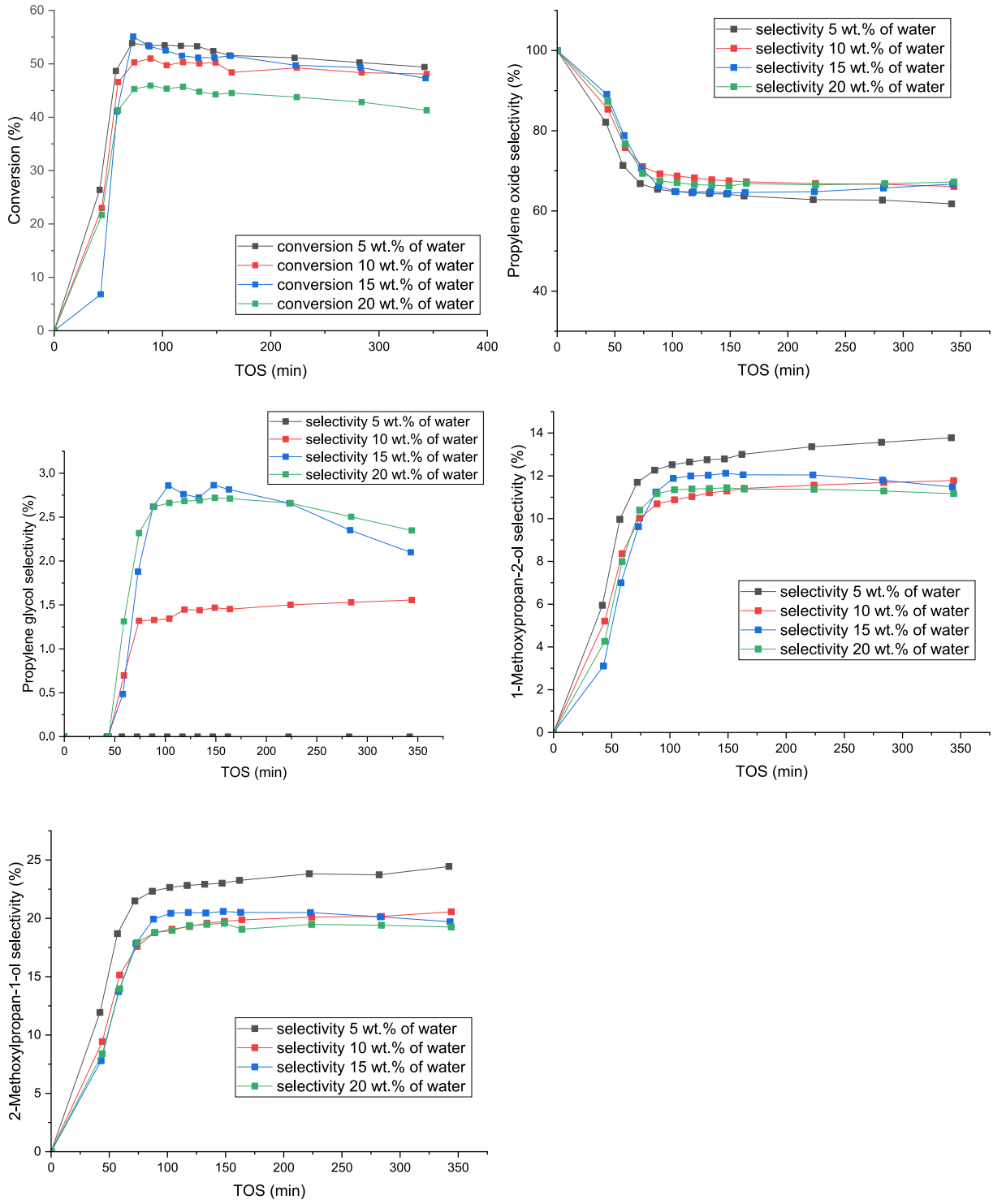

Fig. 12. Effect of water concentration on propylene conversion and product selectivity. Conditions: P = 4.5 bar; T = 40 °C; liquid flow rate = 0.5 ml/min; gas flow rate = 5 ml/min; wt.% H_2O_2 = 2.

Table 6
Estimated kinetic parameters for reactions (1)–(3).

	E_A [kJ/mol]	k'_0 [ ]	K [m^3/mol]
1	42.387	4.097×10^{-1}	5.01×10^{-7}
2	54.067	2.148×10^{-4}	3.87×10^{-6}
3	64.023	3.750×10^{-4}	

$$\frac{k_L a_L d_k^2}{D_{Propylene,L}} = 0.45 X_G^{0.65} Re_L^{1.04} We_L^{0.26} Sc_L^{0.65} \left(\frac{a_v d_k}{1-\varepsilon_B}\right)^{0.325} \quad (17)$$

Equation (17) has several dimensionless parameters, i.e. the Lockhardt-Martinello ratio (X_G), as well as the Reynolds (Re_L), Weber (We_L) and Schmidt (Sc_L) numbers. The last term in equation (17) is basically the description of the characteristics of the catalytic bed. Parameter a_v is the external area of particles and wall per unit reactor volume. Iliuata et al. (Iliuta et al., 1999) have suggested the following equation for estimating

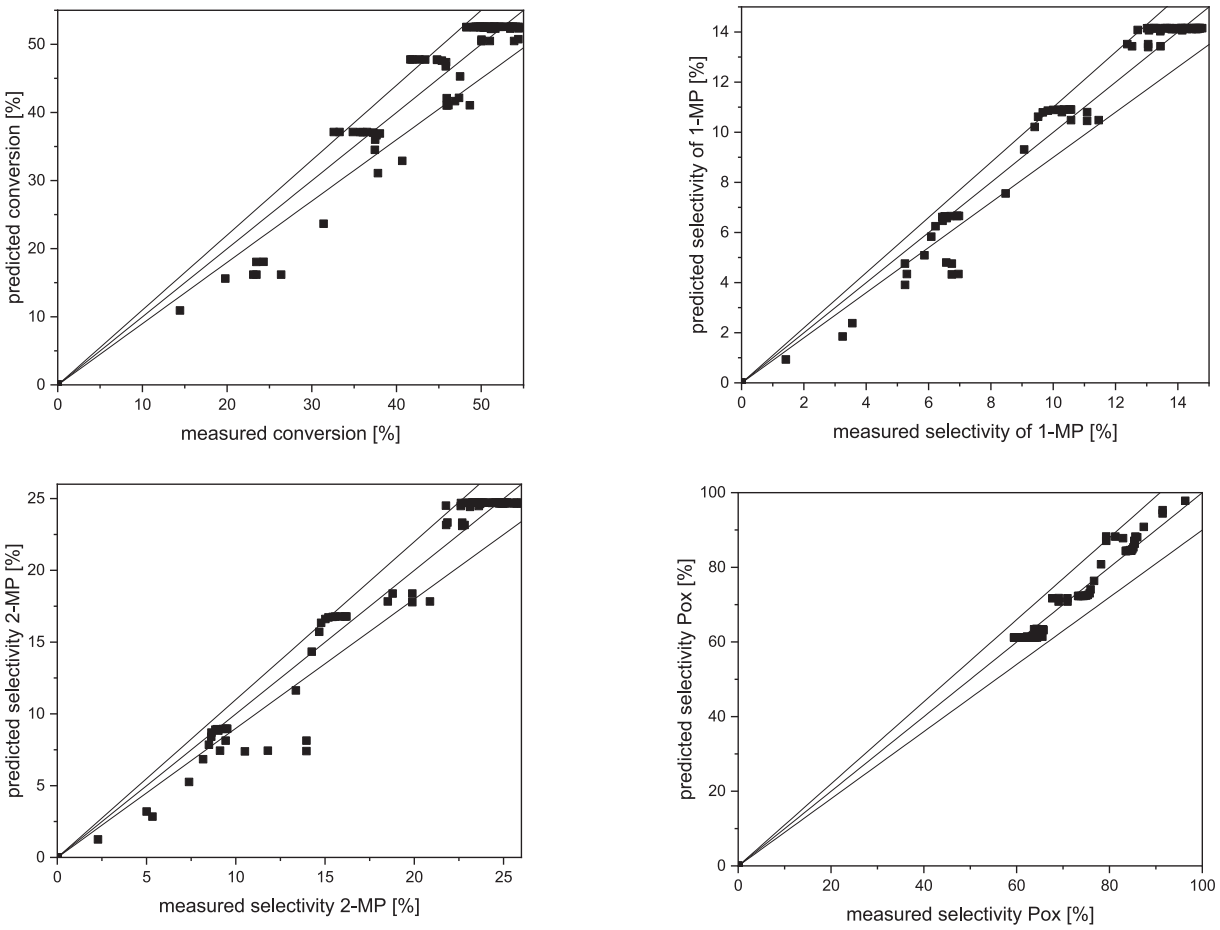

Fig. 13. Parity plots for reference and temperature variation experiments.

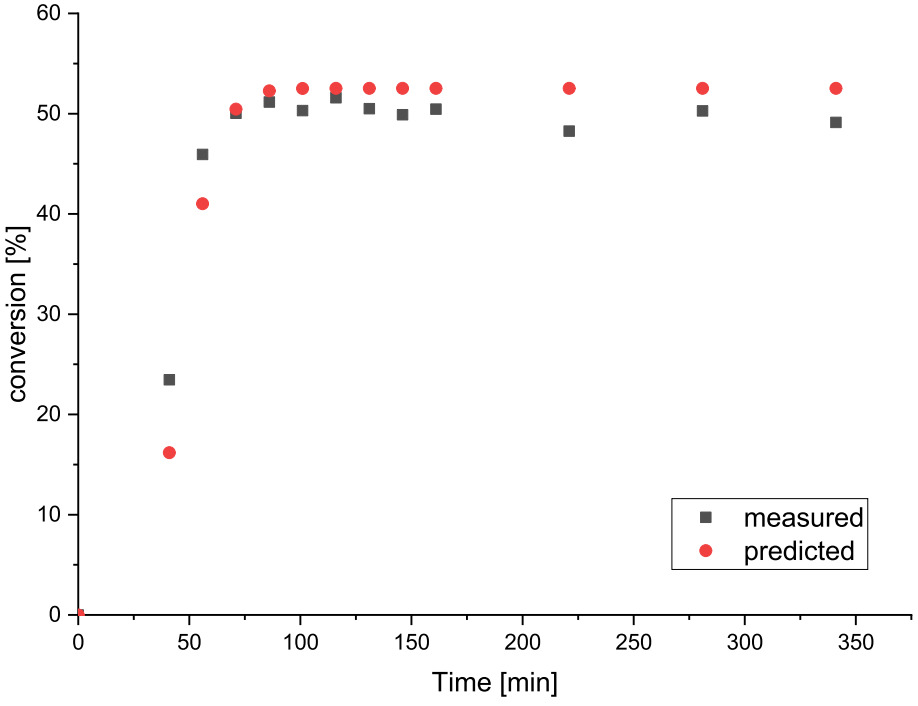

Fig. 14. Measured and predicted propylene conversion in the reference experiment.

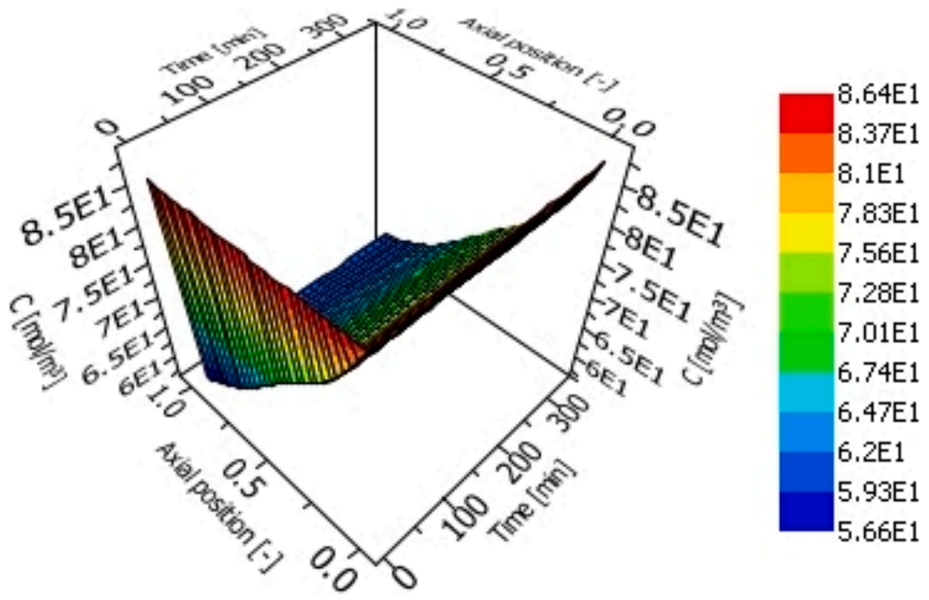

Fig. 15. Concentration of gaseous propylene along the axial position and with time (E0,E1 = 10^0, 10^1 etc).

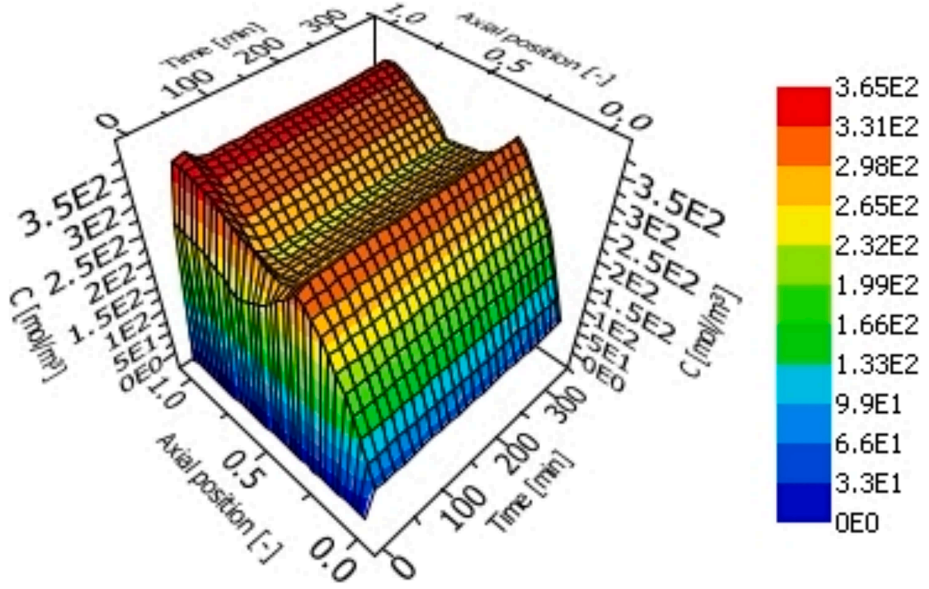

Fig. 16. Concentration of dissolved propylene along the axial position and with time.

this parameter,

$$a_v = \frac{6(1-\varepsilon_B)}{\phi d_p} + \frac{4}{d_R} \tag{18}$$

where Φ is the sphericity factor, which can be assumed to be 0.874 for extrudates and d_R is the reactor diameter.

The Krischer-Kast hydraulic diameter (d_k) in equation (17) is a geometric ratio to take into account the properties of the catalyst itself. It is obtained from equation (19),

$$d_k = d_p \sqrt[3]{\frac{16{\varepsilon_B}^3}{9\pi(1-\varepsilon_B)^2}} \tag{19}$$

where d_p is a volume-based equivalent diameter, which is the diameter of a sphere with the same volume as the extrudate (Iliuta et al., 1999). Assuming that the diameter of the extrudate is 1.5 mm and the length is 12 mm, $d_p = 1.688$ mm.

Liquid-phase mass balance.

The liquid-phase mass balance is shown in equation (20),

$$\varepsilon_L \frac{\partial C_{i,L}}{\partial t} = -\frac{u_L}{L}\frac{\partial C_{i,L}}{\partial \chi} + \varepsilon_L D_{axial,L}\frac{\partial^2 C_{i,L}}{\partial \chi^2} + N_{GL}a_{GL} - \frac{sD_{eff,i}}{R_p}\frac{\partial C_{i,S}}{\partial r_p}\bigg|_{r_p=R_p} \tag{20}$$

Which has basically the same structure as the gas-phase mass balance. The concentration of a compound in the liquid phase is dependent on the convection, the axial dispersion, the gas–liquid flux (gas–liquid mass transfer) and the mass transfer to and from the extrudates.

To describe the axial dispersion effect, it is necessary to estimate the axial dispersion coefficient $D_{axial,L}$. This parameter is calculated from (Azarpour et al., 2021);

$$D_{axial,L} = \frac{u_L d_p}{13{Re_L}^{0.4}{Ga_L}^{-0.33}} \tag{21}$$

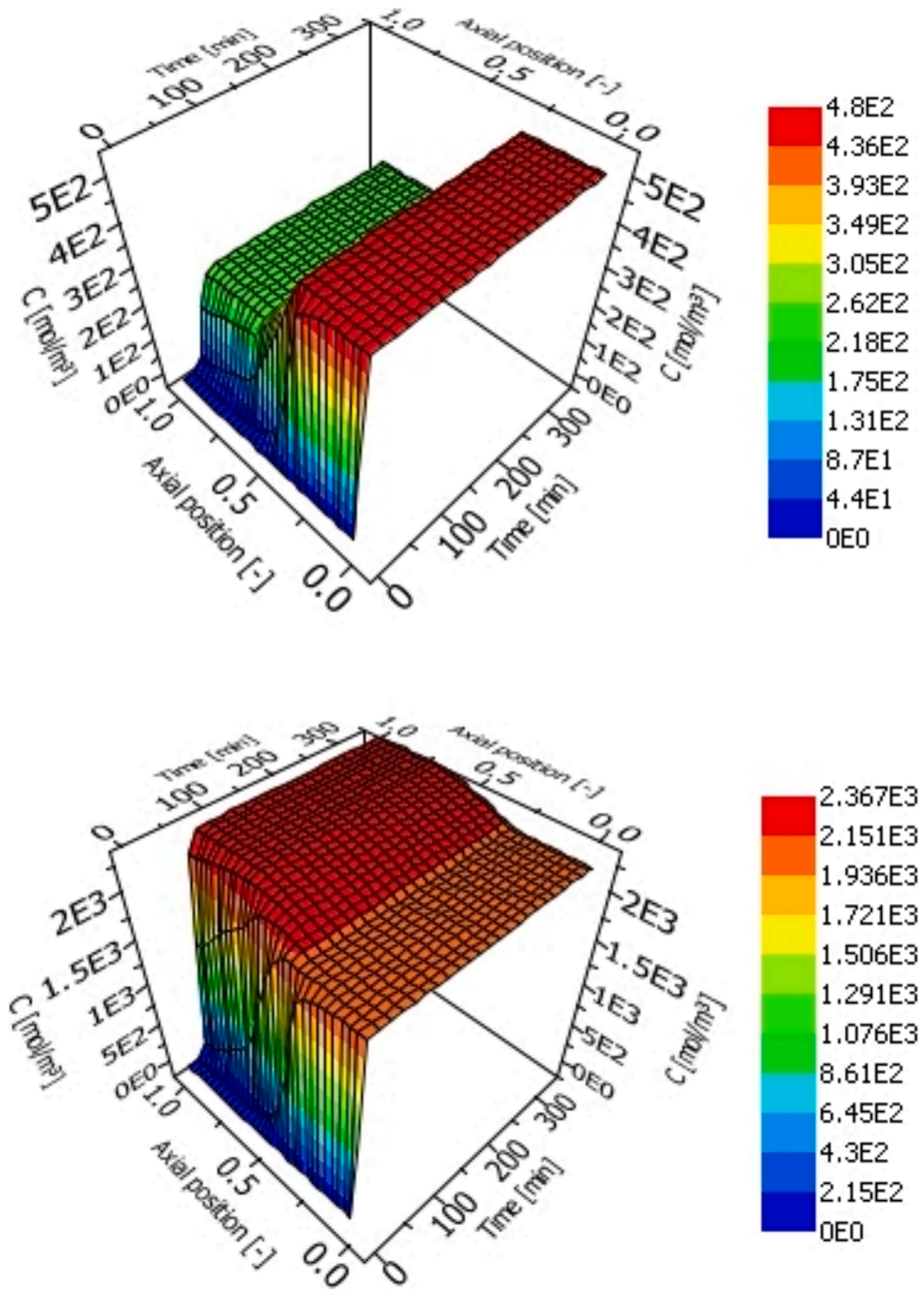

Fig. 17. Hydrogen peroxide (upper) and water (lower) concentrations along the axial position and with time.

The estimation of the Reynolds (Re_L) and Galilei (Ga_L) numbers is based on the extrudate characteristics. In this estimation, the catalyst diameter is standardized by the volumetric equivalent, as described for equation (19).

The approach presented here is different from previous investigations, where the axial dispersion coefficients were estimated from fluid dynamics experiments, i.e. step responses of inert tracers (Alvear et al., 2022; Alvear et al., 2023). These experiments comprised the whole reactor, which is basically filled with inert material (quartz sand), although the chemically active reactor bed is only a small fraction of the system. In the consequence, the measurements give relatively high Péclet numbers (>50) and liquid hold-ups (≈ 45 %), which are not in a good agreement to the expectation based on literature (García-Serna et al., 2017). Therefore, the approach based on available correlations was adopted here.

The mass transfer to/from the solid (liquid–solid flux) is described by the last term of equation (20). The catalyst geometry is taken into the account by the shape factor *s*, the effective diffusion coefficient D_{eff} and the deviation of the concentration on the extrudate surface. The shape factor is obtained from the definition (Aris, 1957; Salmi et al., 2019);

$$s+1=\frac{A_p}{V_p}R_p \tag{22}$$

The shape factor is influenced by the catalyst radius (R_p), the outer surface area of the catalyst (A_p) and the volume of the catalyst particle (V_p). The numerical values of the parameters are listed in Table 2.

The effective diffusion coefficient is estimated with equation (23), based on the mean transport pore model,

$$D_{eff,i}=\frac{\varepsilon_{Cat}}{\tau_{Cat}}D_{A,B} \tag{23}$$

where ε_{Cat} and τ_{Cat} denote the catalyst porosity and tortuosity, respec-

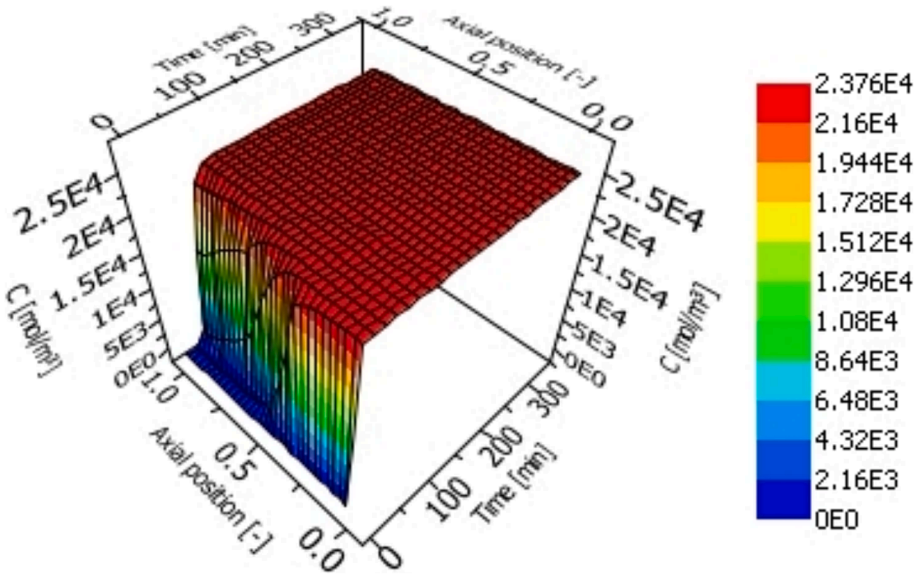

Fig. 18. Methanol concentration along the axial position and with time.

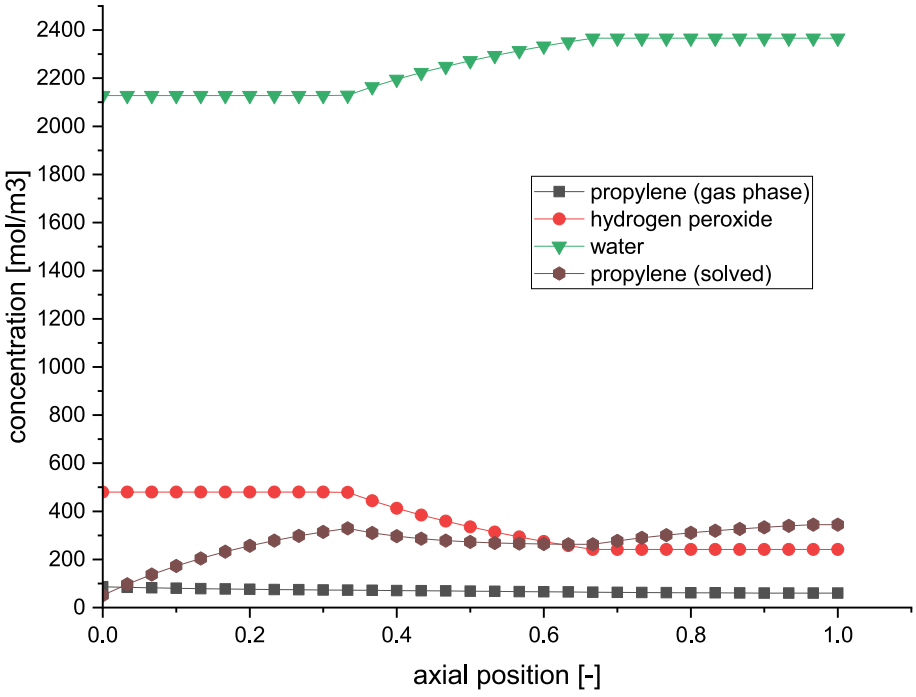

Fig. 19. Concentration profiles of propylene, water and hydrogen peroxide at time = 120 min along the axial position.

tively. For the molecular diffusion coefficient $D_{A,B}$, several correlations have been proposed, the most common being the Wilke-Chang equation (24) (Wilke and Chang, 1955);

$$D_{A,B} = \frac{7.4{*}10^{-12}(\phi_B M_B)^{0.5} T}{\mu_B {*} V_A{}^{0.6}} \tag{24}$$

The association factor of the solvent methanol ($\Phi_B = 1.9$), the molecular weight of the solvent methanol ($M_B = 32.042$ g/mol), the temperature ($T = 313.15$ K), the solvent viscosity ($\mu_{B,313.15K} = 0.454$ cP) and the molar volume of the solute A at its normal boiling point (V_A in cm^3/mol) were used in equation (24). The molar volume parameter was estimated with the method of Schotte (Schotte, 1992), who compared different strategies for the calculation and figured out that the method of Le Bas has a relatively high error (Reid et al., 1959). The following empirical equation has been suggested to obtain more accurate estimates,

$$V = 0.32L(L-1) + \sum A_j G_j \tag{25}$$

Parameter L describes the chain length, A_j is the number of groups j in the molecule and G_j is the relative compound group with a specific value. Table 3 summarizes the values for the molar volumes of the reactants at the boiling point for the calculation of the diffusion coefficient $D_{A,B}$ for each compound present in the liquid phase.

To estimate the effective diffusive coefficients, the catalyst porosity ε_{Cat} and the tortuosity τ_{Cat} are estimated. Based on nitrogen physisorption, the catalyst porosity can be approximated to $\varepsilon_{Cat} = 0.31$. The tortuosity can be calculated with different equations depending on the

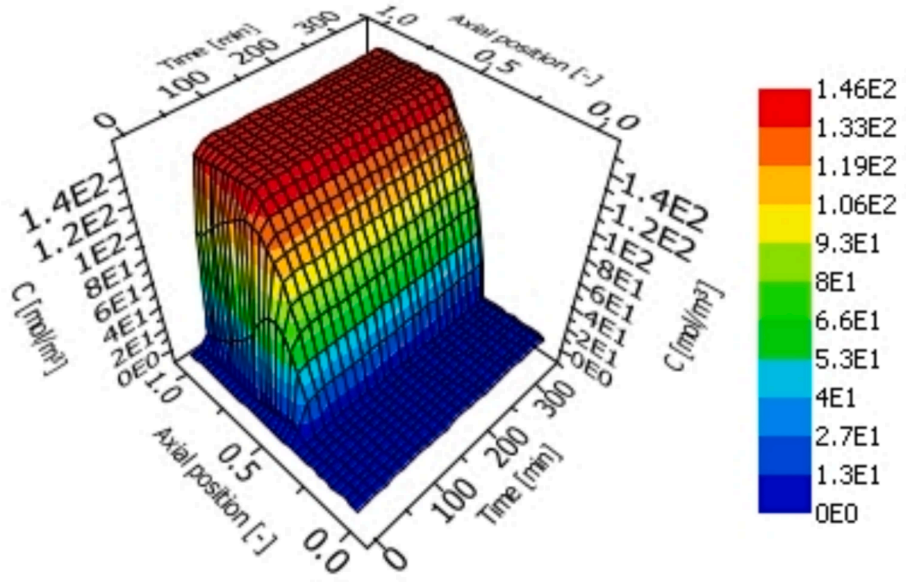

Fig. 20. Propylene oxide concentration along the axial position and with time.

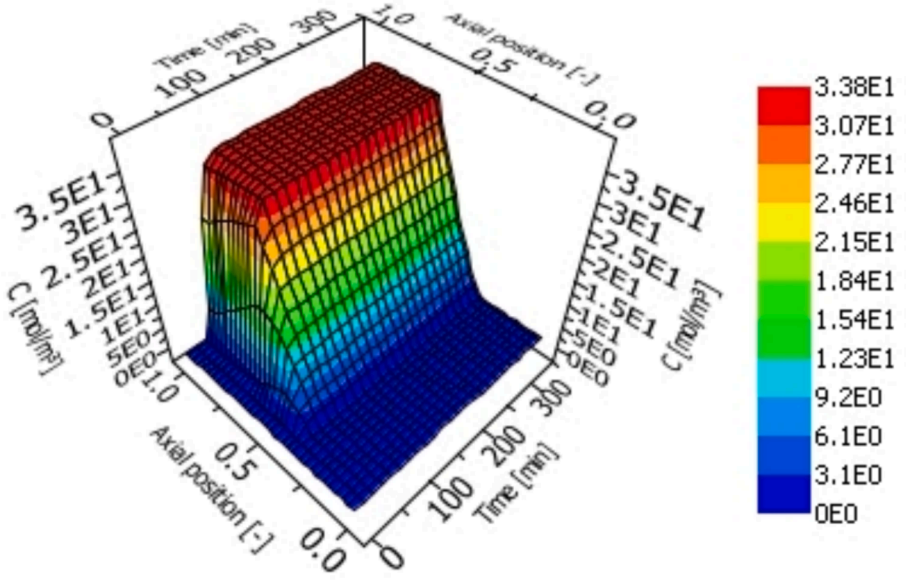

Fig. 21. 1-methoxypropan-2-ol concentration along the axial position and with time.

catalyst shape. Kolitcheff et al. (Kolitcheff et al., 2017) has provided a good overview on different methods. Equation (26) for random homogenous isotropic sphere packings was used in this work be used to estimate the tortuosity (Akanni et al., 1987).

$$\tau_{Cat} = \frac{3 - \varepsilon_{Cat}}{2} \tag{26}$$

According to the above equation, $\tau_{Cat} = 1.35$ for the TS-1 extrudates.

Solid-phase mass balance.

The solid-phase mass balance is expressed as

$$\frac{\partial C_{i,s}}{\partial t} = \frac{D_{eff,i}}{\varepsilon_S}\left(\frac{\partial^2 C_{i,s}}{\partial r_P{}^2} + \frac{s}{r_P}\frac{\partial C_{i,S}}{\partial r_p}\right) + \rho_B \frac{\varepsilon_L}{\varepsilon_S}\sum \nu_{i,j} r_j \tag{27}$$

This equation describes the diffusion inside the pores of the catalyst particle and the intrinsic reaction kinetics on the active sites on the catalyst surface.

Initial and boundary conditions.

After the mass balance equations for the gas, liquid and solid phases have been defined, it is important to set initial and boundary conditions to solve the coupled system of partial and ordinary differential equations (PDE-ODEs). The inlet to the reactor ($\chi = 0$) is characterized by the feed concentration of each substance in the gas and liquid phases. For the gas phase, plug flow behavior was presumed, but for the liquid phase, the impact of axial dispersion is considered. Consequently, the inlet boundary conditions can be written as follows,

$$c_{i,G} = c_{0i,G}\chi = 0 \tag{28}$$

$$\frac{D_{axial}}{L}\frac{dc_{i,L}}{d\chi}\bigg|_{\chi=0} = -u\left(c_{0i,L} - c_{i,L}\big|_{\chi=0}\right) \qquad \chi = 0 \tag{29}$$

The axial concentration gradients disappear at the reactor outlet ($\chi = 1$) according to the closed boundary condition of Danckwerts (Danckwerts,

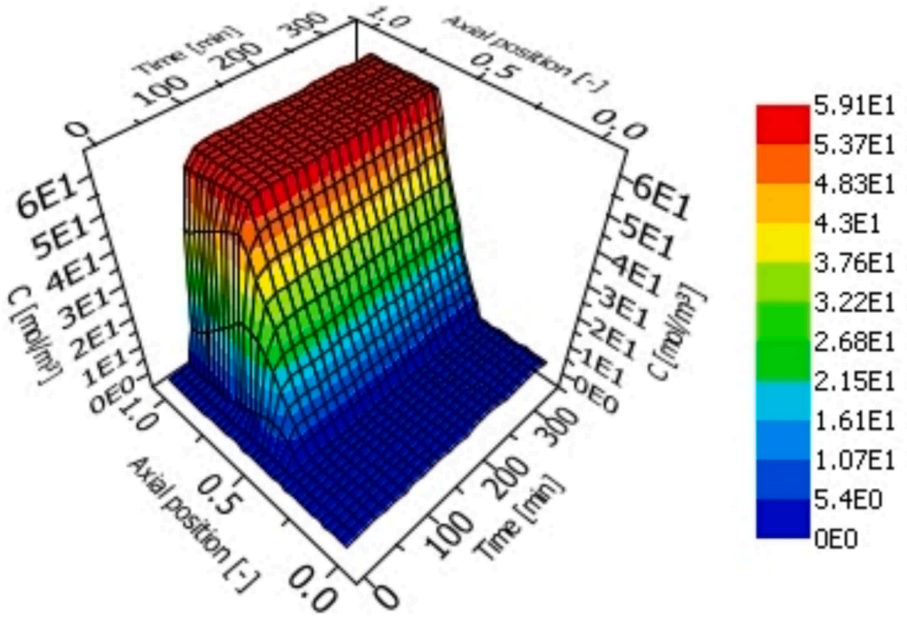

Fig. 22. 2-methoxylpropan-1-ol concentration along the axial position and with time.

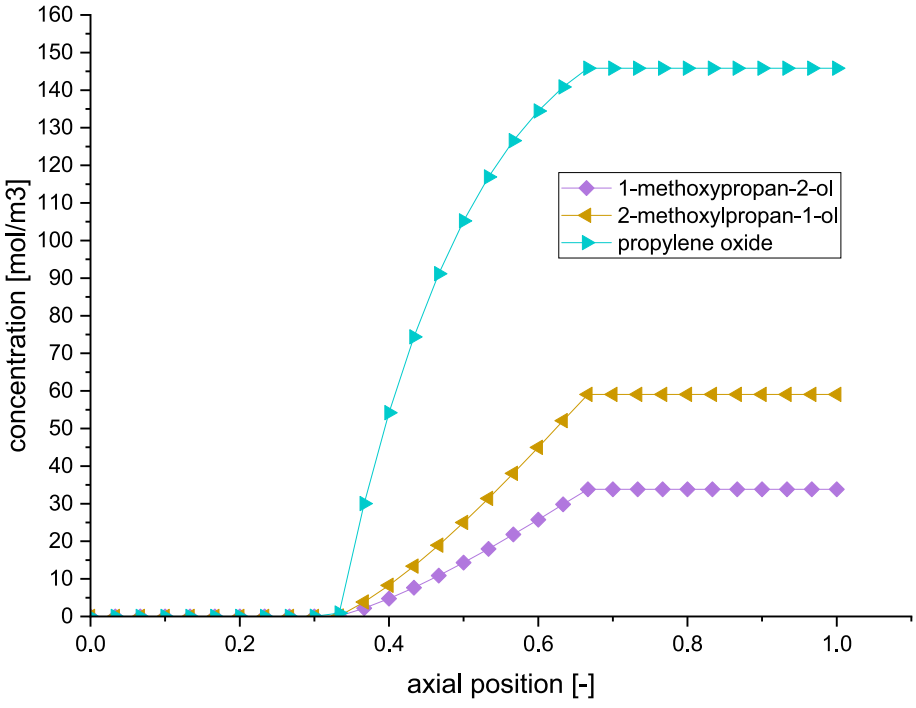

Fig. 23. Concentration profiles of 1-methoxypropan-2-ol, 2-methoxylpropan-1-ol and propylene oxide at time = 120 min along the axial position.

Table 7
Concentration gap between the liquid bulk phase and the extrudates.

Compound	Concentration in the bulk phase [mol/m^3]	Concentration on the particle rim [mol/m^3]	Wetting efficiency [-]
propylene	310.49	306.04	0.99
methanol	23754.50	23751.60	1.00
hydrogen peroxide	443.97	429.41	0.97
water	2163.93	2176.12	0.99
propylene oxide	30.00	50.67	0.59
1-methoxypropan-2-ol	2.19	3.45	0.63
2-methoxylpropan-1-ol	3.83	6.44	0.59

Axial position = 0.3667, time = 120 min

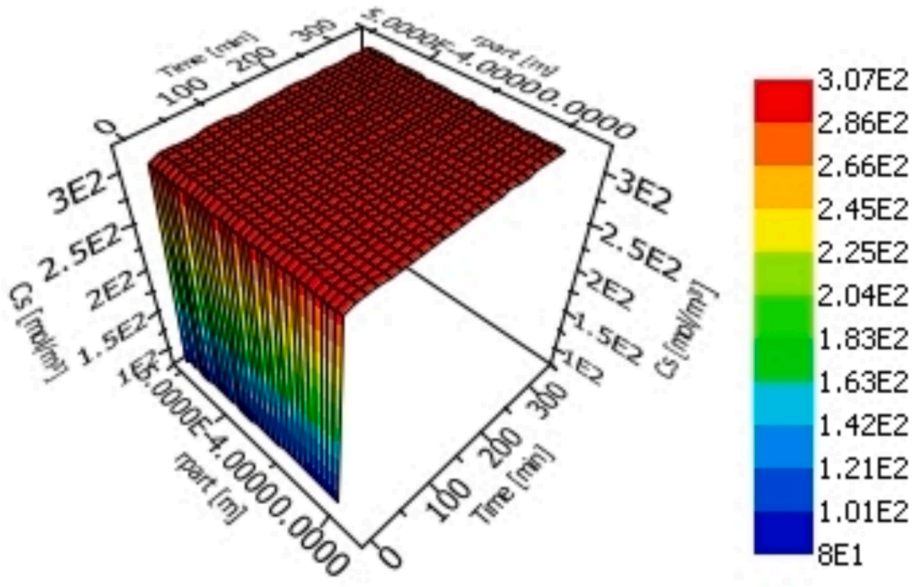

Fig. 24. Propylene concentration along the particle radius and with time (axial position = 0.3667).

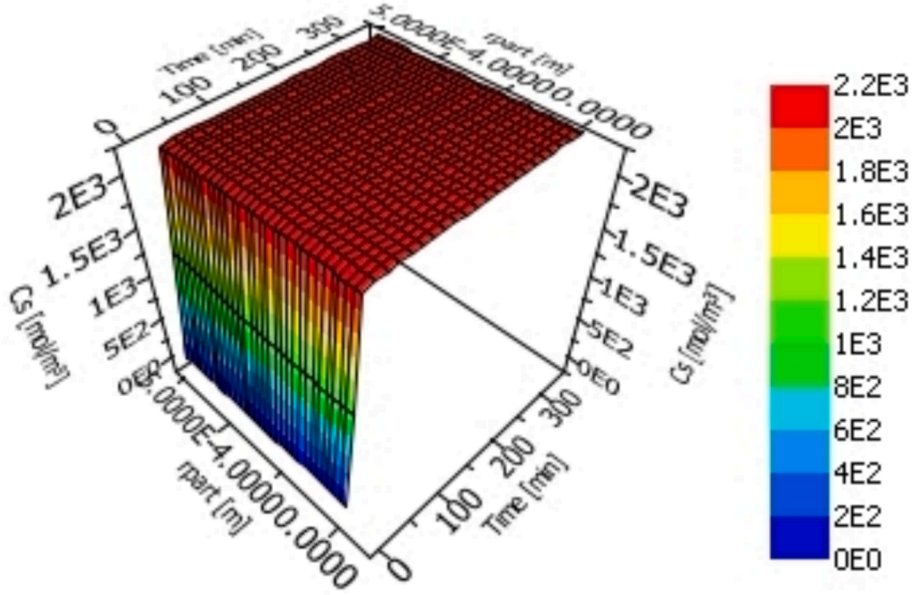

Fig. 25. Water concentration along the particle radius and with time (axial position = 0.3667).

1953);

$$\frac{\partial c_{i,G}}{\partial \chi} = 0 \qquad \chi = 1 \tag{30}$$

$$\frac{\partial c_{i,L}}{\partial \chi} = 0 \qquad \chi = 1 \tag{31}$$

By considering the external mass transfer from/to the outer surface of the catalyst particle and the diffusion flux from/to the catalyst, the boundary condition at the outer surface of the catalyst becomes

$$\frac{s}{R_p} D_{eff,i} \frac{\partial C_{i,S}}{\partial r_p}\bigg|_{r_p=R_p} = k_{i,LS}\xi_{ls}\left(c_{i,L} - c_{i,L}\big|_{r_p=R_p}\right) \tag{32}$$

The liquid–solid phase interphase parameter ξ_{ls} is approximated with equation (33) (Iliuta et al., 1999).

$$\xi_{ls} = \frac{6(1-\varepsilon_B)}{\phi d_p} + \frac{4}{d} \tag{33}$$

where Φ is the sphericity factor for the cylindrical extrudates, $\Phi = 0.874$. Equation (33) gives the interfacial area parameter $\xi_{ls} = 2946\ m^2/m^3$ which is in a good agreement with the expected value (Trambouze and Euzen, 2002).

The value of the mass transfer coefficient $k_{i,LS}$ needed in equation (32) was calculated with the approximation (34) proposed by Satterfield et al. (Satterfield et al., 1978).

$$\frac{k_{LS} d_p}{D_{A,B}} \frac{a_W}{a_P} = 0.815 Re_L^{0.822} \left(\frac{\mu_L}{\rho_L D_{A,B}}\right)^{0.333} \tag{34}$$

Equation (34) shows that the main parameters which can affect the mass transfer coefficient are the particle diameter (d_p) as well as the liquid

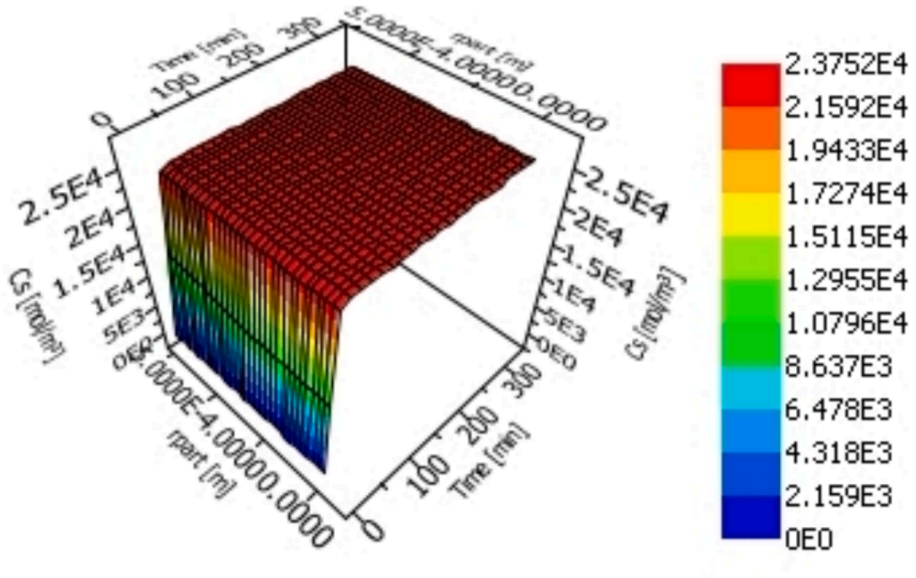

Fig. 26. Methanol concentration along the particle radius and with time (axial position = 0.3667).

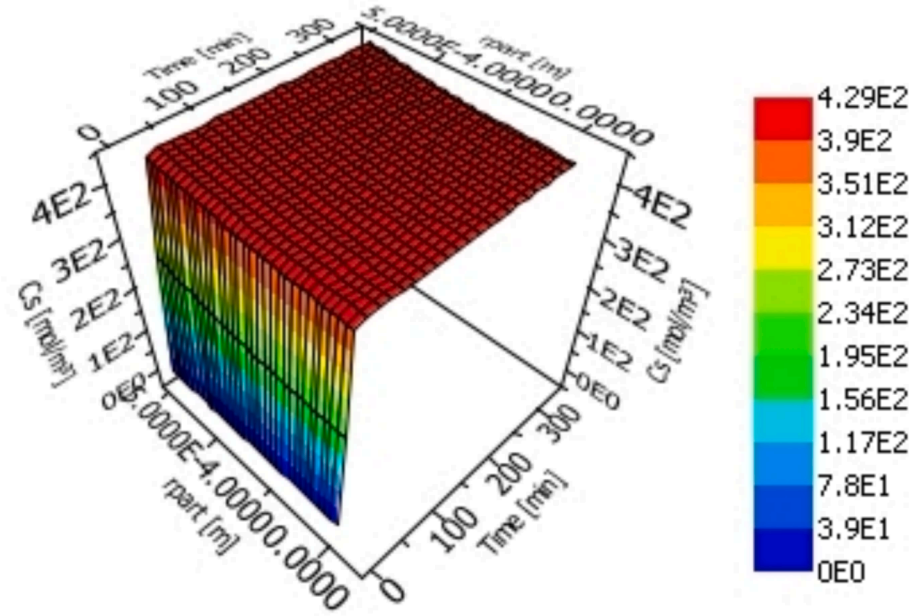

Fig. 27. Hydrogen peroxide concentration along the particle radius and with time (axial position = 0.3667).

velocity, which is included in the Reynolds number (Re_L). The mass transfer resistance can be suppressed by using small particles and high liquid velocities. The ratio between the external wetted area (a_W) and the external area of particle (a_P) can be adjusted by a wetting efficiency factor. It is assumed that this value is 0.7 based on previous studies (Alvear et al., 2023). A summary of the boundary conditions is provided below.

$c_{i,S} = c_{0i,L}$ $\chi = 0$ at the reactor entrance (35).

$\frac{\partial C_{i,S}}{\partial \chi} = 0$ $\chi = 1$ at the reactor outlet (36).

$\frac{s}{R_p} D_{eff,i} \frac{\partial C_{i,S}}{\partial r_P} = k_{i,LS} \xi_{LS} \left(C_{i,L} - C_{i,S}{}^{Rp} \right)$ $r_P = R_p$ at the particle surface (37).

$\frac{\partial C_{i,S}}{\partial r_P} = 0$ $r_P = 0$ at the particle centre because of symmetry reasons (38).

Physical properties estimation and numerical strategies.

For the calculation of the dimensionless numbers included in the model, the estimation of the liquid-phase properties is necessary. The estimation was carried out by *AspenPlus* for the reaction conditions. The properties of the gas phase were described the ideal gas law. Henry's constant was defined as the ratio between the concentration of propylene in the gas and the liquid phases; it was estimated by a flash model with the aid of *AspenPlus*.

The model equations were solved numerically with the software *gProms ModelBuilder v.6.0.2*. The equations represented a system of strongly coupled partial (PDE) and ordinary differential equations (ODE). The approach of the software is to discretize the differential equations with respect to the spatial coordinates. In this way, the original system of ODEs and PDEs is converted to a large system of ODEs, an initial value problem, which is solved as a function of time. Backward finite difference formulae were used for the discretization and a spatial grid of 30 points was applied. For the parameter estimation, the software

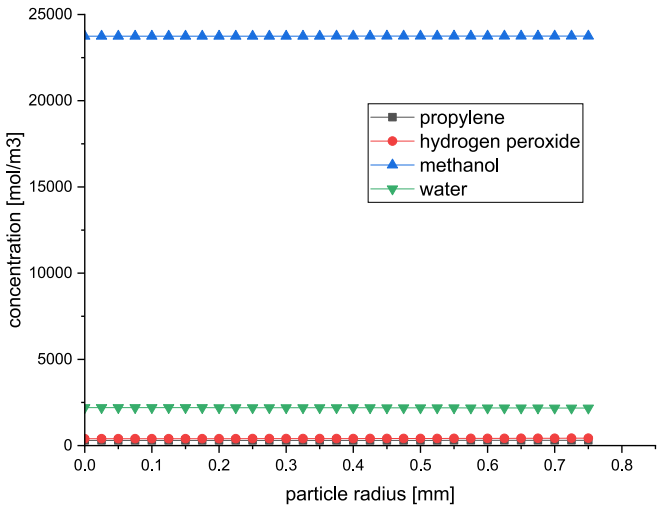

Fig. 28. Concentration profiles of methanol, propylene, water and hydrogen peroxide at time = 120 min, axial position = 0.3667 along the particle radius.

used a solver called "MXLKHD". This solver is based on the maximum likelihood approach, which means that the solver tries to maximize the predictability of the experimental data with the aid of the model equations.

4. Experimental results and discussion

4.1. Preliminary study of catalyst performance

The preliminary kinetic studies with the catalysts were conducted to understand the influence of the physical dimensions of the catalyst extrudates on the epoxidation process. It was expected that the extrudate size should have an effect because previous studies with catalyst powders have indicated the presence of internal mass transfer limitations (Alvear et al., 2022; Alvear et al., 2023).

4.1.1. Catalyst activity and selectivity

One of the aims of this work was to figure out, which one of the catalyst extrudates might show the highest propylene conversion and the highest propylene oxide selectivity. The check the catalyst durability and the experimental reproducibility, each experiment was repeated. The results are displayed in Fig. 3.

The reproducibility of the experiments was high: the data points from of the repeated experiments coincided. Fig. 3a) shows that the propylene conversion increases with smaller extrudate diameters. The highest conversion level (45 %) was reached with the catalyst with the smallest diameter, but the conversion decreased (30 %) for the 3.5 mm diameter extrudate. Evidently the internal diffusion limitations play an important role in the reaction system and they should be taken into the account in mathematical modelling. Fig. 3b) confirms that the epoxide selectivity is independent of the catalyst particle diameter. Each sample gave approximately the same selectivity (60 %). It is important to emphasize that the conversion level (90 %) and the epoxide selectivity (75 %) are much lower for the extrudates compared to the results obtained for a powder catalyst (Alvear et al., 2021). Based on the results of these preliminary experiments, the 1.5 mm diameter extrudate was selected for further experiments and for the development of the mathematical model.

4.1.2. Nitrogen physisorption

Table 4 gives the results of the nitrogen physisorption measurements.

The measurements revealed that the surface area of the extrudates varied between 259 and 418 m^2/g. Comparing the fresh and spent catalysts, it is noticeable that in most of the samples, the surface area of the fresh catalyst is slightly higher than the spent one. The reason for this could be that some reaction products block the pores in the spent catalysts. An exception of this observation is the extrudate with 2.5 mm in diameter. It is interesting to notice that the surface area of the extrudate with 1.5 mm in diameter decreased from 418 m^2/g to 223 m^2/g. It is however important to remember that this catalyst was a part of the investigation of the effect of ammonia on the epoxidation process, so it might be possible that some of the pores became blocked by ammonia.

The pore volume varied within a wide range from 0.028 cm^3/g to 0.133 cm^3/g. The fresh extrudates with 2.5 mm and 1.5 mm had the largest pore volumes, while the spent samples and the other extrudates showed much smaller pore volumes. The smallest extrudate had the highest microporous volume 0.202 cm^3/g. for the other samples, the microporous volume varied between 0.104 cm^3/g and 0.154 cm^3/g. The

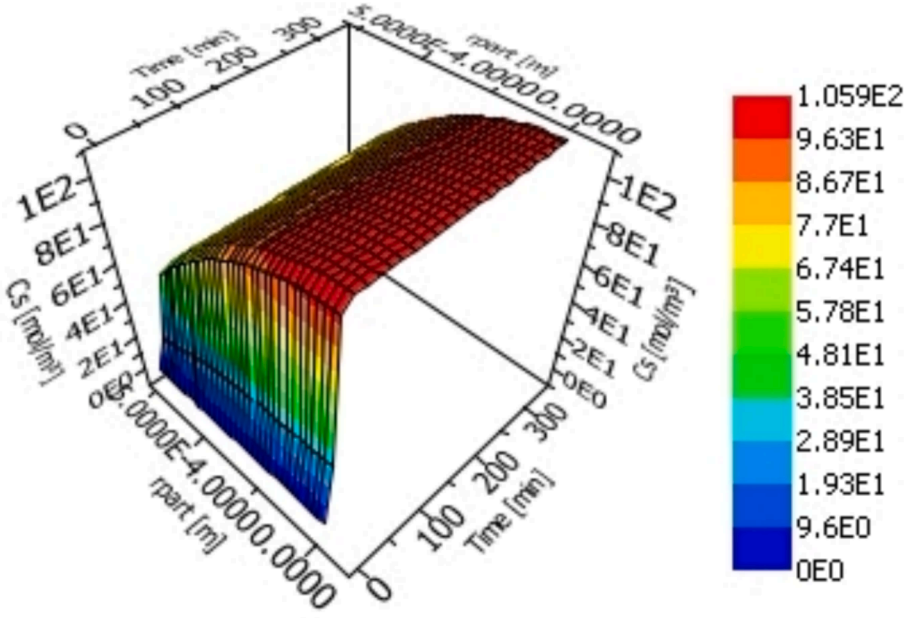

Fig. 29. Propylene oxide concentration along the particle radius and with time (axial position = 0.3667).

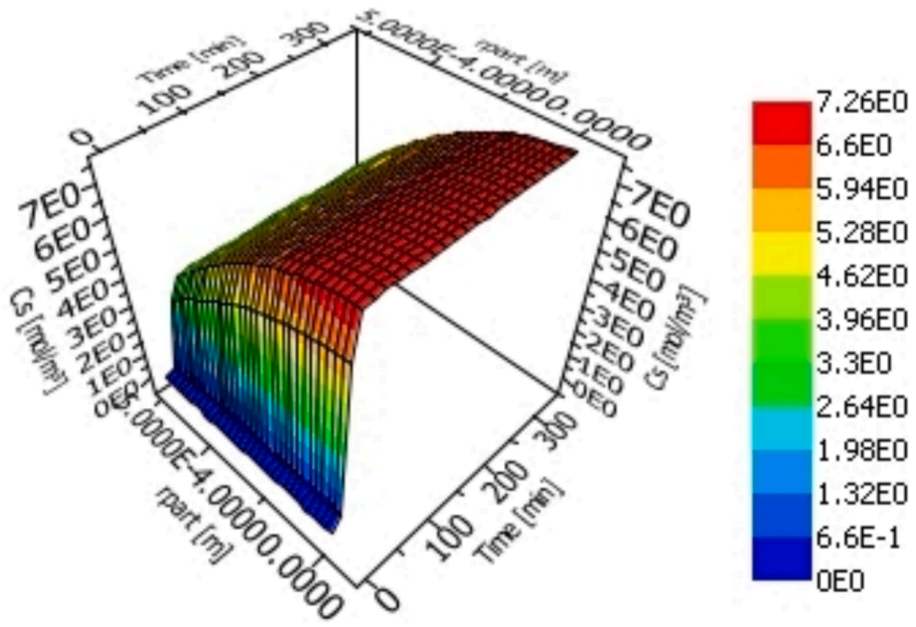

Fig. 30. 1-methoxypropan-2-ol concentration along the particle radius and with time (axial position = 0.3667).

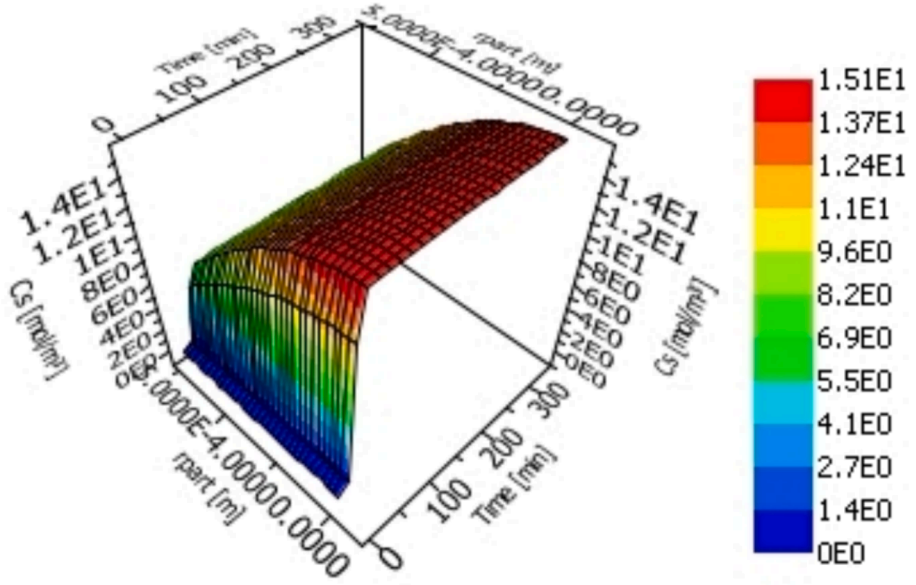

Fig. 31. 2-methoxylpropan-1-ol concentration along the particle radius and with time (axial position = 0.3667).

only parameter, which was approximately the same for all the samples, was the average pore diameter around 0.622 nm.

The observed data are in a good accordance with the information obtained from previous investigations on TS-1 powder and synthesized Ti-MWW catalysts with highly crystalline structures and with high Ti amounts (Alvear et al. 2024).

4.1.3. Scanning electron microscopy (SEM-EDS)

The SEM-EDS technique was used for two reasons: SEM highlights visible differences between fresh and used extrudates and EDS indicates, if there are changes in the catalyst morphology caused by the reaction or the cleaning process at elevated pressure (6.5 bar) and temperature (70 °C).

The main results of this investigation are displayed in Fig. 4. All the compared images did not show any visible changes on the surface structure. The spherical shape of the crystals was preserved and the diameter of the spheres were basically the same. This result suggests a good mechanical stability of the catalyst during the reaction and during the cleaning process.

The analysis results of the surface composition obtained with EDS are summarized in Table 5, confirming that the composition of all the extrudates had the same elemental composition.

It is necessary to emphasize that the molar ratio of the main compounds SiO_2 and TiO_2 is much higher compared to previous investigations (Alvear et al. 2024), which indicates that a higher amount of titanium exists inside the catalyst structure, affecting the number of available active sites and the acidity as well.

4.1.4. Temperature programmed desorption (TPD)

The results of the TPD measurements are summarized in Fig. 5. The results confirm that the catalyst acidities were approximately between 5 and 11 mmol/g. The acidities of the extrudates were more than five

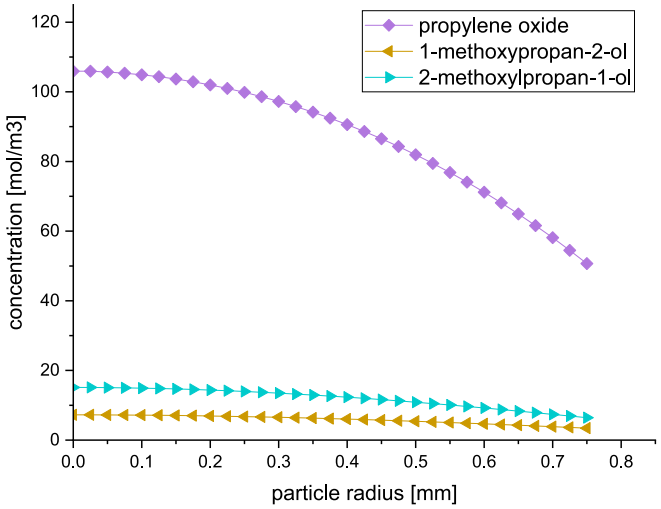

Fig. 32. Concentration profiles of 1-methoxypropan-2-ol, 2-methoxylpropan-1-ol and propylene oxide at time = 120 min, axial position = 0.3667 along the particle radius.

times higher than observed for the catalyst powder (Alvear et al. 2024). This result is less surprising, regarding the higher amount of titanium present in the extrudates. It is also noticeable that the spent catalysts had a higher acidity than the fresh ones. The explanation could be that some hydrogen peroxide remains adsorbed on the catalyst surface even after the cleaning process, which leads to the formation of titanium hydroxide species (Belussi et al., 1992; Bonino et al., 2004). Bonino et al. have investigated the effect of these sites on the acidity, and they observed a decreasing pH-value, i.e. increasing acidity in the presence of the titanium hydroxide species compared to the measurement results obtained for a fresh TS-1 catalyst (Bonino et al., 2004).

4.1.5. X-ray diffraction (XRD)

The XRD diffractograms displayed in Fig. 6 confirm that all the samples had the same composition as the diffraction patterns are very similar. The main compounds are titanium silicon oxide (ICSD 90712) and anatase (ICSD 121632, marked with stars). Evidently no irreversible phase transformations had taken place during the kinetic experiments. The analysis reveals as well that the crystallinity of the samples is very high, because no amorphous backgrounds are visible in the diffractograms.

4.2. Effect of operation parameters

The effect of different reaction conditions on the catalyst performance was investigated with systematic experiments using the 1.5 mm catalyst extrudates. The experimental parameters studied were temperature, pressure, liquid flow rate, propylene flow rate as well as the water and hydrogen peroxide concentrations.

4.2.1. Temperature effect

The effect of the temperature was investigated at 20, 30 and 40 °C because temperatures exceeding 50 °C could promote the hydrogen peroxide decomposition (Alvear et al., 2021). It was expected that with an increasing temperature, the propylene conversion would increase as well. This assumption was confirmed by the experimental observations displayed in Fig. 7.

The average conversion was around 51 % at 40 °C and decreased to 36 % at 20 °C. The propylene oxide (PO) selectivity increased with a lower temperature, which is clearly visible in Fig. 7. Increasing the temperature promotes the ring opening reactions, resulting in higher amounts of 1-methoxypropan-2-ol (1-MP) and 2-methoxylpropan-1-ol (2-MP). These results are in a good accordance with previous investigations (Alvear et al., 2021; Alvear et al., 2023). It is evident that the activation energies of the ring-opening reactions are higher than the activation energy of the epoxidation reaction.

4.2.2. Effect of liquid flow rate

The liquid flow rate of the H_2O_2 solution was changed from 0.5 ml/min up to 2 ml/min. Based on previous investigations, it was expected that the propylene conversion decreases, the propylene oxide selectivity increases and the 1-MP and 2-MP selectivities decrease with a higher flow rate (Alvear et al., 2021; Alvear et al., 2023). This assumption could be not fully proven in the present investigation. Fig. 8 shows that the highest propylene conversion (51 %) was reached at the volumetric flow rate 0.5 ml/min, but the highest selectivity of approximately (78 %) was achievable at the flow rate 2 ml/min.

Interestingly, the conversion level was lower with the flow rate 1.5 ml/min than with 2 ml/min. An explanation could be based on the consideration of the effect of a higher flow rate. Increasing the liquid flow leads to a decreasing of the residence time, but in the trickle bed reactor, the liquid flow influences the wetting efficiency. Therefore, the wetting efficiency increases with a higher liquid flow rate. Even though the residence time decreases, the wetting efficiency and therefore the local amount of hydrogen peroxide increases, which can lead to a higher conversion (Azarpour et al., 2021).

4.2.3. Pressure effect

The variation of the pressure was studied at 2.5 bar, 4.5 bar and 6.5 bar. By increasing the pressure, the propylene solubility in the liquid phase increases. It was supposed that the conversion might therefore increase as well, as it is shown in Fig. 9. The propylene oxide selectivity increased, while the 1-MP and 2-MP selectivities decreased smoothly. This effect was investigated in a previous investigation, and the present results are in a good accordance with these studies (Alvear et al., 2021).

4.2.4. Effect of propylene flow rate

The effect of the propylene flow rate was investigated within the range 5–10 ml/min. It was observed that the propylene conversion was strongly decreasing, as the propylene flow was decreasing. The results displayed in Fig. 10 are comparable to previous investigations (Alvear et al., 2021). However, the propylene oxide selectivity was approximately the same for the different propylene flow rates, which contradicts previous work conducted with powder catalysts. In addition, the total gas flow rate was increasing with increasing the amount propylene, which results in a lower residence time of the gas-phase molecules, thus suppressing the further reactions.

4.2.5. Effect of hydrogen peroxide concentration

The variation of the hydrogen peroxide concentration did not have an effect on the propylene conversion. The conversion was for the concentrations 2—6 wt% approximately the same as shown in Fig. 11. The propylene oxide selectivity had an interesting behavior, because the value decreased from 61 % to 54 % as the H_2O_2 amount was decreased from 4 wt% to 6 wt%. The 1-MP and 2-MP selectivities increased with the higher amounts of H_2O_2, even though a higher amount of H_2O_2 than 4 wt% did not have an impact. The selectivities of the side products were approximately 17 % (1-MP) and 29 % (2-MP) at the steady state. Evidently a higher amount of H_2O_2 than 4 wt% did not have an effect on the selectivity anymore.

4.2.6. Effect of water concentration

Considering the reaction scheme displayed in Fig. 1, a higher amount of water in the educt solution should lead to a higher amount of propylene glycol because of the ring opening reaction. To investigate this effect, the amount of water was varied in the range between 4.7–20 wt %. The results are presented in Fig. 12.

The experimental results indicated that the conversion level is independent of the water, until 20 wt%. The propylene oxide selectivity

was approximately the same in all the experiments. The propylene glycol selectivity was not increasing that much, as could have been expected based on previous investigations (Alvear et al., 2021). The amount of propylene glycol was always under 3 %, while the propylene oxide selectivity was not decreasing. The higher amount of water resulted basically in a smooth decrease of the 1-MP and 2-MP selectivities. The results were somewhat surprising. It was expected that the amount of propylene glycol might increase with a higher amount of water but for 15 wt% and 20 wt%, the results were basically similar.

5. Modelling results and discussion

5.1. Parameter estimation results

The model was expected to be a precise approach to the interaction of kinetic and mass transfer effects in a trickle bed reactor. The challenge is the complexity of the model, which makes the parameter estimation sometimes difficult. To reach the convergence of the estimation process, the initial values of the parameters must be close to the final solution. In this case it was necessary to estimate eight parameters simultaneously. The approach was to estimate first the parameters, which are valid for the reference experiments (40 °C, 4.5 barg, $\dot{n}_{C_3H_6} = 0.223\text{mmol/min}$, $\dot{V}_{H_2O_2} = 0.5ml/min$, $w_{H_2O_2} = 2wt.\%$, $w_{H_2O} = 4.7wt.\%$). After this initial attempt, these values were fixed and the experiments with different temperatures were used to evaluate the activation energies. The results of this approach are summarized in Table 6.

The initial values for the parameter estimation were obtained from literature (Danov et al., 2013). The final result of the parameter estimation of the activation energy and adsorption constant are in a good accordance to the values reported by Danov et al. (Danov et al., 2013). The model predictions are in a quite good agreement with the experimental data, which is visible in the parity plots collected in Fig. 13.

Fig. 13 indicates that the model underestimates the values in the low percentage area. It is possible that the mass transfer limitations are not yet considered precisely enough. A typical progress of the propylene conversion is given in Fig. 14. The two first predicted data points have some deviation compared to the experimental points at the steady state. This behavior was observable both in the conversion as well as the selectivity plots.

It can be summarized that the model describes most of the experimental data within the range of +/- 10 % deviation at the steady state for the reference and temperature variation experiments.

Considering the description of the mass transfer effects, a noticeable improvement was achieved. Previous publications often claimed that the mass transfer limitations play a role in the system, but the effect was neglected in the modelling. In the present approach, this phenomenon included in the modelling effort. Therefore, the first data points are better predicted.

5.2. Model evaluation

The main aim is to investigate the concentration profiles in the reactor tube and inside the catalyst extrudates. The estimated parameters were used in the numerical simulations to elucidate the behavior of the system.

5.2.1. Concentration profiles along the reactor tube

The concentration profile of propylene in the gas phase is illustrated in Fig. 15. As expected, the propylene concentration decreases along the reactor length. This phenomenon is driven by two effects: propylene dissolves in the liquid phase and the dissolved. propylene in the liquid phase is consumed by the epoxidation reaction. It should be highlighted that at the beginning ($t = 0$ min), the reactor is assumed to be completely filled with propylene, which is a reasonable initial condition, since gaseous propylene enters the reactor space rapidly.

In contrast to the propylene in the gas phase, it was expected that the dissolved propylene should have a different concentration profile. The concentration in the liquid phase is mainly affected by continuous mass transfer of propylene from the gas to the liquid phase and by the epoxidation reaction. Therefore, the model should show a continuous increase of propylene in the liquid phase, except in the catalytic bed. In consideration of the reactor setup, only 1/3 of the reactor was filled with the catalyst extrudates. The space before and after the catalyst bed was filled with inert material as described in Experimental Section. Exactly the expected behavior is visible in Fig. 16. The propylene amount in the liquid phase increases in the first part of the reactor system. In the catalyst bed, a decreasing tendency is visible because of the reaction, which means that the reaction is more rapid than the dissolution process. In the last part of the reactor, the amount of dissolved propylene increases again because the reaction rate retards.

The other main educt for the epoxidation is hydrogen peroxide, which is consumed in the catalytic bed during the reaction. Because of the small amount of hydrogen peroxide (2 wt%) in the liquid phase, it was expected that a concentration drop would be visible, as confirmed by the simulations displayed in Fig. 17. An analogous but opposite behavior was expected for the water concentration (4.7 wt%), because it is the stoichiometric co-product of the reaction. The model can predict this behavior very well, too.

The methanol concentration is affected by the ring-opening reactions to 1-MP and 2-MP (Fig. 1). The amount of methanol is enormous in comparison to the other educts, being 93 wt% in the reference experiments. The high amount leads to the expectation that the concentration profile should be practically constant along the axial position, as confirmed in Fig. 18.

The findings are illustrated in Fig. 19, where the concentrations of gas-phase and dissolved propylene, hydrogen peroxide and water along the axial reactor coordinate at the steady state are displayed. Methanol is not shown in the figure because of the very high concentration compared to the other compounds.

In case of the reaction products, it was expected that the concentrations will increase only in the catalytic bed, but not varying before and after the reaction zone. This behavior is visible in Figs. 20-22.

Fig. 23 confirms that the expected concentration ratios are predicted by the mathematical model. Therefore, the highest product concentration is reached for propylene oxide. The 1-MP and 2-MP concentrations are on a lower level.

5.2.2. External mass transfer effects

After the discussion of the bulk liquid phase, it is necessary to have a closer look at the interaction between the liquid phase and the catalyst particles. The investigation was carried out at a reference point in the catalyst bed under steady state conditions, which are shown in Table 7.

Table 7 confirms that the concentrations of the educts are higher in the bulk phase than on the outer surface of the particle, which was expected because of external mass transfer limitations. Analogously, the concentration of the products is higher on the particle rim than in the bulk liquid phase. The results are in a good agreement with the expectations that molecules with a bigger size have higher concentration gradients because of the lower diffusion coefficient and higher diffusion resistance.

5.2.3. Internal mass transfer – concentration profiles along the particle

The reference point for the discussion of internal mass transfer effects is the first data point inside the catalytic bed, which is given by the model (dimensionless axial coordinate = 0.3667). This data point was selected to illustrate the system at a relatively low, but still noticeable propylene conversion (Fig. 23). In case of methanol, propylene and water, the concentration gradients inside the extrudate are very modest as illustrated in Figs. 24-26. Similar observations were made for the other axial points.

Because the reactor is basically filled with the educt solution and the

amount of products is not that high in comparison to the educts, it is expected that no mass transfer limitations are visible, and the pores of the extrudates are basically filled with the compounds from the educt solution. This is confirmed for hydrogen peroxide in Fig. 27, although a very smooth concentration decrease along the particle radius is noticeable.

Fig. 28 shows more precisely that the concentrations of the compounds in the reactor feed are not changing inside the catalyst particles itself.

For the products it was expected that concentration gradients might be visible, which is confirmed by Figs. 29-31. The product concentrations are low in the vicinity of the outer surface of the extrudate and high inside the particle with an increasing trend along the radius. This behavior is one of the main reasons for the time delay in the transient state in the beginning of the experiments: the diffusion of the products out of the catalyst particle can be slow. Fig. 32 illustrates how the concentration of the product propylene oxide is changing faster than in case of the other products. This is in a good accordance with the expectations (Aquino et al., 2023; Wu et al., 2008; van der Waal and van Bekkum, 1997).

5.2.4. Summary of the model evaluation

The aim of the modelling approach was to describe the real system in a more advanced way. The model comprises the macroscopic scale, e.g. reactor characterization involving hold-ups as well as the consideration of mass transfer limitations on the microscopic scale. The work demonstrated that this aim was fulfilled. Especially, the concentration profiles of the compounds along the axial position and the particle radius are meaningful. This argumentation is based on parameters, which were estimated with the aid of the reference and temperature variation experiments. A further investigation with very wide boundary ranges of the estimated parameters and all experiments showed that the selectivity courses are quite stable which is related to stable kinetic constants. Apart from that, the conversion courses showed a higher deviation from experimental data, which is mainly related to the adsorption constants because they were changing a lot during the parameter estimation. Another reason could be the impact of mass transfer. It was mentioned that the model cannot predict the first data point very well. It is always necessary to keep in mind that the mass transfer limitations were evaluated with equations obtained from available literature. Because of the very low flow velocities applied in the current work, these equations might not be completely valid. The best way to reach a higher precision is to measure experimentally these values for the given system, Only when the intrinsic reaction kinetics is absolutely clear, it is possible to measure the mass transfer parameters in a reliable way (Dang-Vu et al., 2006) (Banchero et al., 2004).

6. Conclusions

TS-1 extrudates with four different diameters were prepared and characterized with nitrogen physisorption, SEM-EDS, TPD and XRD. The catalysts were used for propylene epoxidation in the laboratory-scale trickle bed reactor. The extrudates with the smallest diameter of 1.5 mm showed the highest propylene conversion to propylene oxide because of noticeable internal mass transfer limitations were present in the larger extrudates. Characterization of the extrudates before and after the reaction did not reveal any fundamental changes in the catalyst properties. A deeper study of the smallest catalyst extrudate (diameter 1.5 mm) was carried out since this catalyst had the best performance. The propylene conversion was increased with increasing pressure, temperature and decreasing the liquid flow rate, propylene flow rate and keeping the amount of water in the solution under 20 %. The epoxide selectivity increased with decreasing temperature, the amount of hydrogen peroxide in the solution and increasing liquid flow rate.

It was noticed that the conversion and selectivity were changing slowly in prolonged experiments. An explanation for the deactivation might be the formation of bigger molecules, which block the catalyst pores (Russo et al., 2014; Thiele and Roland, 1997). The original activity was restored after a cleaning procedure.

The generated experimental database was used for the estimation of the model parameters. The simplified approach of the reaction kinetics allowed more advanced consideration of the mass transfer limitations of the catalyst extrudates. The gas–liquid and the liquid–solid mass transfer coefficients as well as the axial dispersion coefficients and the holdups were estimated from available correlations.

7. Future perspectives

To improve the model, as many parameters as possible.should be measured experimentally. For example, the detailed characterization of the fluid dynamics gives room for improvement in the estimation of the liquid holdup and the axial dispersion coefficient.

The impact of the mass transfer coefficients is crucial. Most of the existing correlation equations are valid at higher flow velocities, so it is meaningful to adjust these parameters. With the aid of corrector factors, it is possible to adapt the coefficients to the system, but the danger lies in masking the extrapolation error. The recommendable way to surmount this dilemma is to measure these parameters for the actual system. The existing literature gives some suggestions to measure and approximate the wetting efficiency with residence time distribution experiments, investigation of the pressure drop, computed tomography, calorimetry and dye absorption as well as computational fluid dynamics (CFD) (Azarpour et al., 2021; Ranade et al., 2011; Julcour-Lebigue et al., 2009).

An extension of the present model is possible by including catalyst deactivation. It was noticed that the conversion and selectivity were changing slowly in prolonged experiments. An explanation for the reversible deactivation might be the formation of bigger molecules, which block the catalyst pores (Russo et al., 2014; Thiele and Roland, 1997), but the original activity was restored after a cleaning procedure. A time-dependent deactivation equation could be added to the model, to describe the decline of the catalyst activity (Kilpiö et al., 2016).

CRediT authorship contribution statement

Christopher Stäglich: Writing – original draft, Visualization, Validation, Methodology, Formal analysis, Data curation, Conceptualization. **Matias Alvear:** Validation. **Christoph Schmidt:** Supervision, Project administration, Methodology, Investigation, Conceptualization. **Ilari Angervo:** Visualization, Validation, Formal analysis, Data curation. **Vincenzo Russo:** Supervision, Software, Investigation, Formal analysis, Conceptualization. **Stefan Haase:** Supervision, Methodology, Conceptualization. **Tapio Salmi:** Writing – original draft, Supervision, Resources, Methodology, Investigation, Funding acquisition, Formal analysis, Conceptualization.

Declaration of competing interest

The authors declare that they have no known competing financial interests or personal relationships that could have appeared to influence the work reported in this paper.

Acknowledgement

This work is part of the activities of Johan Gadolin Process Chemistry Centre (PCC) at Åbo Akademi University. Economic support from Academy of Finland, through the Academy Professor grants 319002, 345053 (Tapio Salmi, Matias Alvear) is gratefully acknowledged.

Appendix A. Supplementary data

Supplementary data to this article can be found online at https://doi.

org/10.1016/j.ces.2025.121570.

Data availability

Data will be made available on request.

References

M. P. G. N. B. Taramasso, Preparation of porous crystalline synthetic material comprised of silicon and titanium oxides, US Patent 4410501, 1983.

Russo, V., Tesser, R., Santacesaria, E., Di Serio, M., 2013. Chemical and technical aspects of propene oxide production via hydrogen peroxide (HPPO process). Ind. Eng. Chem. Res. 52, 1168–1178. https://doi.org/10.1021/ie3023862.

Bassler, P., Weidenbach, M., Goebbel, H.-G., 2010. The New HPPO Process for Propylene Oxide: from Joint Development to Worldscale Production. Chem. Eng. Trans. 21, 571–576. https://doi.org/10.3303/CET1021096.

Alvear, M., Reich, M.-L., Eränen, K., Haase, S., Murzin, D., Salmi, T., 2023. Molecular structure effect on the epoxidation of 1-butene and iso-butene on titanium silicate catalyst under transient conditions in a trickle bed reactor. ACS Omega 8, 25710–25726. https://doi.org/10.1021/acsomega.3c00087.

Alvear, M., Eränen, K., Murzin, D.Y., Salmi, T., 2021. Study of the product distribution in the epoxidation of propylene over TS-1 catalyst in a trickle bed reactor. Ind. Eng. Chem. Res. 60, 2430–2438. https://doi.org/10.1021/acs.iecr.0c06150.

Liu, X., Wang, X., Guo, X., Li, G., 2004. Effect of solvent on the propylene epoxidation over TS-1 catalyst. Catal. Today 93–95, 505–509. https://doi.org/10.1016/j.cattod.2004.06.077.

Alvear, M., Fortunato, M.E., Russo, V., Salmi, T., Di Serio, M., 2022. Modelling of transient kinetics in trickle bed reactors: Ethylene oxide production via hydrogen peroxide. Chem. Eng. Sci. 248, 117156. https://doi.org/10.1016/j.ces.2021.117156.

Alvear, M., Orabona, F., Eränen, K., Lehtonen, J., Rautiainen, S., Di Serio, M., Russo, V., Salmi, T., 2023. Epoxidation of light olefin mixtures with hydrogen peroxide on TS-1 in a laboratory-scale trickle bed reactor: Transient experimental study and mathematical modelling. Chem. Eng. Sci. 269, 118467. https://doi.org/10.1016/j.ces.2023.118467.

Azarpour, A., Rezaei, N., Zendehboudi, S., 2021. Performance analysis and modeling of catalytic trickle bed reactors: a comprehensive review. J. Ind. Eng. Chem. 103, 1–41. https://doi.org/10.1016/j.jiec.2021.04.020.

Influence of Si/Ti ratio and calcination conditions, 2024. M. Alvear, C. Schmidt, O. Reinsdorf, E. Lebron-Rodrigez, A. Al Abdulghan, I. Hermans, M. Peurla, M. Lastusaari, K. Eränen, D. Murzin, N. Kumar., Ti-MWW catalysts for propylene oxide production. Catal. Lett. 154, 834–845. https://doi.org/10.1007/s10562-023-04350-x.

Belussi, G., Carati, A., Cleici, M.G., Maddinelli, G., Millini, R., 1992. Reactions of titanium silicalite with protic molecules and hydrogen peroxide. J. Catal. 133, 220–230. https://doi.org/10.1016/0021-9517(92)90199-R.

Bonino, F., Damin, A., Ricchiardi, G., Ricci, M., Spanò, G., D'Aloisio, R., Zecchina, A., Lamberti, C., Prestipino, C., Bordega, S., 2004. Ti-Peroxo species in the TS-1/H_2O_2/H_2O system. J. Phys. Chem. B 108, 3573–3583. https://doi.org/10.1021/jp036166e.

Ranade, V.V., Chaudhari, R., Gunjal, P.R., 2011. Trickle Bed Reactors. Reactor Engineering and Applications, First Edition, Elsevier, Amsterdam.

Al-Dahhan, M.H., Larachi, F., Dudukovic, M.P., Laurent, A., 1997. High-pressure trickle bed reactors: A Review. Ind. Eng. Chem. Res. 36, 3292–3314. https://doi.org/10.1021/ie9700829.

Russo, V.; Kilpiö, T.; Di Serio, M.; Tesser, R.; Santacesaria, E.; Murzin, D. Yu.; Salmi, T., Dynamic non-isothermal trickle bed reactor with both internal diffusion and heat conduction: Sugar hydrogenation as a case study Chemical Engineering Research and Design 102 (2015), 171-185, doi:/10.1016/j.cherd.2015.06.011.

Hachhach, M., Russo, V., Murzin, D.Y., Salmi, T., 2023. Dynamic modelling of trickle bed reactor: Case study of arabinose oxidation. Powder Technol. 425, 118608. https://doi.org/10.1016/j.powtec.2023.118608.

Danov, S.M., Sulimov, A.V., Kolesnikov, V.A., Ovcharov, A.A., 2013. Kinetics of propylene epoxidation with hydrogen peroxide. Kinet. Catal. 54, 193–198. https://doi.org/10.1134/S0023158413020031.

Russo, V., Tesser, R., Santacesaria, E., Di Serio, M., 2014. Kinetics of propene oxide production via hydrogen peroxide with TS-1. Ind. Eng. Chem. Res. 53 (15), 6274–6287. https://doi.org/10.1021/ie404271k.

Aquino, A., Korup, O., Horn, R., 2023. Liquid phase epoxidation of propylene to propylene oxide with hydrogen peroxide on titanium silicalite-1: Spatially resolved measurements and numerical simulations. Ind. Eng. Chem. Res. 62, 3098–3115. https://doi.org/10.1021/acs.iecr.2c03373.

Wu, Y., Liu, Q., Su, X., Mi, Z., 2008. Effect of solvents on propylene epoxidation over TS-1 catalyst. Front. Chem. Chin. 3, 112–117. https://doi.org/10.1007/s11458-008-0007-2.

van der Waal, J.C., van Bekkum, H., 1997. Zeolite titanium beta: A versatile epoxidation catalyst. Solvent effects. J. Mol. Catal. A Chem. 124, 137–146. https://doi.org/10.1016/S1381-1169(97)00074-5.

A. Corma, P. Esteve, and A. Martínez, Solvent effects during the oxidation of olefins and alcohols with hydrogen peroxide on Ti-Beta catalyst: The influence of the hydrophilicity–hydrophobicity of the zeolite, Journal of Catalysis 161, 11–19, 1996, doi: 10.1006/jcat.1996.0157.

Dudukovic, M.P., Kuzeljevic, Ž.V., Combest, D.P., 2014. Three-phase trickle-bed reactors, in Ullmann's Encyclopedia of Industrial Chemistry. Wiley 1–40. https://doi.org/10.1002/14356007.b04_309.pub2.

Pushnov, A.S., 2006. Calculation of average bed porosity. Chem. Pet. Eng. 42, 14–17. https://doi.org/10.1007/s10556-006-0045-x.

Lange, R., Schubert, M., Bauer, T., 2005. Liquid holdup in trickle bed reactors at very low liquid Reynolds numbers. Ind. Eng. Chem. Res. 44, 6504–6508. https://doi.org/10.1021/ie048906r.

García-Serna, J., Gallina, G., Biasi, P., Salmi, T., 2017. Liquid holdup by gravimetric recirculation continuous measurement method. Application to Trickle Bed Reactors under Pressure at Laboratory Scale, Industrial and Engineering Chemistry Research 56, 13294–13300. https://doi.org/10.1021/acs.iecr.7b01810.

T. Chang, R. M. Rousseau, and J. K. Ferrell, Vapor/liquid equilibria of constituents from coal gasification in refrigerated methanol, United States Environmental Agency, EPA/600/7-87/004, 1987.

Gianetto, A., Specchia, V., 1992. Trickle bed reactors: state of art and perspectives. Chem. Eng. Sci. 47, 3197–3213. https://doi.org/10.1016/0009-2509(92)85029-B.

Ellman, M., 1988. Caractéristiques des réacteurs triphasés à lit fixe fonctionnant à co-courant vers le bas. Thèse de doctorat, Nancy INPL.

Iliuta, I., Larachi, F., Grandjean, B.P.A., Wild, G., 1999. Gas–liquid interfacial mass transfer in trickle bed reactors: state-of-the-art correlations. Chem. Eng. Sci. 54, 5633–5645. https://doi.org/10.1016/S0009-2509(99)00129-3.

Aris, R., 1957. On shape factors for irregular particles—I. Chem. Eng. Sci. 6, 262–268. https://doi.org/10.1016/0009-2509(57)85028-3.

Salmi, T., Mikkola, J.-P., Wärnå, J., 2019. Chemical Reaction Engineering and Reactor Technology, Second Edition. CRC Press Taylor & Francis Group, Boca Raton, Florida.

Wilke, C.R., Chang, P., 1955. Correlation of diffusion coefficients in dilute solutions. AIChE J 1, 264–270. https://doi.org/10.1002/aic.690010222.

Schotte, W., 1992. Prediction of the molar volume at the normal boiling point. The Chemical Engineering Journal 48, 167–172. https://doi.org/10.1016/0300-9467(92)80032-6.

Reid, R.C., Sherwood, T.K., Street, R.E., 1959. The Properties of Gases and Liquids. Phys. Today 12, 38–40. https://doi.org/10.1063/1.3060771.

Kolitcheff, S., Jolimaitre, E., Hugon, A., Verstraete, J., Carrette, P.-L., Tayakout-Fayolle, M., 2017. Tortuosity of mesoporous alumina catalyst supports: Influence of the pore network organization. Microporous Mesoporous Mater. 248, 91–98. https://doi.org/10.1016/j.micromeso.2017.04.010.

Akanni, K.A., Evans, J.W., Abramson, I.S., 1987. Effective transport coefficients in heterogeneous media. Chem. Eng. Sci. 42, 1945–1954. https://doi.org/10.1016/0009-2509(87)80141-0.

Danckwerts, P.V., 1953. Continuous flow systems. Chem. Eng. Sci. 2, 1–13. https://doi.org/10.1016/0009-2509(53)80001-1.

Trambouze, P., Euzen, J.-P., 2002. Les réacteurs chimiques – De la conception á la mise en oeuvre. Editions Technip, Paris.

Satterfield, C.N., Van Eek, M.W., Bliss, G.S., 1978. Liquid-solid mass transfer in packed beds with downward concurrent gas-liquid flow. AIChE J 24, 709–717. https://doi.org/10.1002/aic.690240421.

Dang-Vu, T., Doan, H.D., Lohi, A., 2006. Local Mass Transfer in a Packed Bed: Experiments and Model. Ind. Eng. Chem. Res. 45, 1097–1104. https://doi.org/10.1021/ie0505312.

Banchero, M., Manna, L., Sicardi, S., Boelhouwer, J.G., Urseanu, M.I., Kwant, G., 2004. Conversion rate and mass transfer limitation in trickle bed reactors in the presence of a fast reaction. Chem. Eng. Sci. 59, 5411–5416. https://doi.org/10.1016/j.ces.2004.08.017.

Julcour-Lebigue, C., Augier, F., Maffre, H., Wilhelm, A.-M., Delmas, H., 2009. Measurements and modeling of wetting efficiency in trickle bed reactors: Liquid viscosity and bed packing effects. Ind. Eng. Chem. Res. 48, 6811–6819. https://doi.org/10.1021/ie9002443.

Thiele, G.F., Roland, E., 1997. Propylene epoxidation with hydrogen peroxide and titanium silicalite catalyst: Activity, deactivation and regeneration of the catalyst. Journal of Molecular Catalysis a: Chemica 117, 351–356. https://doi.org/10.1016/S1381-1169(96)00266-X.

T. Kilpiö, V. Russo, K. Eränen, and T. Salmi, Design and modeling of laboratory scale three-phase fixed bed reactors, Physical Sciences Reviews 1(3), 2016, doi: 10.1515/psr-2015-0020.